

1

INTRODUCTION

SUPERFLUIDS are liquids and gases with remarkable properties. In particular, superfluid helium can flow through a capillary without friction due to its extremely small viscosity (at least 1500 times smaller than normal liquid helium^[1]), or creep up the wall of a container, seemingly defying the force of gravity^[2] (“Rollin creeping”). Its thermal conductivity is about 3×10^6 times higher than that of liquid helium I or about 200 times higher than that of copper at room temperature^[3]. It therefore earned the title of “best heat conducting substance we know” by Willem and his daughter Anna Keesom and dubbed “*supra-heat-conducting*”^[3]. Later it was understood why^[4–7] and it turns out that heat does not diffuse through the medium as in normal liquids, but rather it travels through the medium in waves (second sound). This makes it an ideal coolant e.g. to stabilise the superconducting magnets in CERN’s Large Hadron Collider^[8]. Helium is also the only known substance that stays liquid at zero temperature and low pressures and both its angular momentum and vorticity are quantised, making it the first observed macroscopic quantum substance. Helium-4 becomes superfluid below the λ -point, named so by William H. Keesom in 1936 who measured a singularity in the specific heat at $T_\lambda = 2.2\text{ K}$ ^[3].

1.1 A BRIEF HISTORY OF SUPERFLUIDITY

Helium was the last gas to be liquefied and was done so by Heike Kamerlingh Onnes in 1908^[11,12]. In 1932 John McLennan saw that liquid helium stopped boiling below $\approx 2.2\text{ K}$ ^[13] and later that year Willem Keesom and his daughter Anna observed, while measuring the temperature dependence of the specific heat, a singularity around the same temperature^[9]. They called it the “ λ -temperature”, T_λ , because of the shape of the temperature dependence of the specific heat resembling the Greek letter λ (see Figure 1.1). A few years later in 1935 Burton measured a sharp decrease in the viscosity of liquid helium below T_λ ^[14]. Around the same time Fritz London was already thinking about macroscopic wave functions and why helium does not freeze at $T = 0\text{ K}$ under atmospheric pressure^[15]. London and Simon concluded that it was caused by the zero point motion of the helium atoms and their associated kinetic energy that is comparable to their Van der Waals energy, effectively preventing liquid helium to solidify^[16,17].

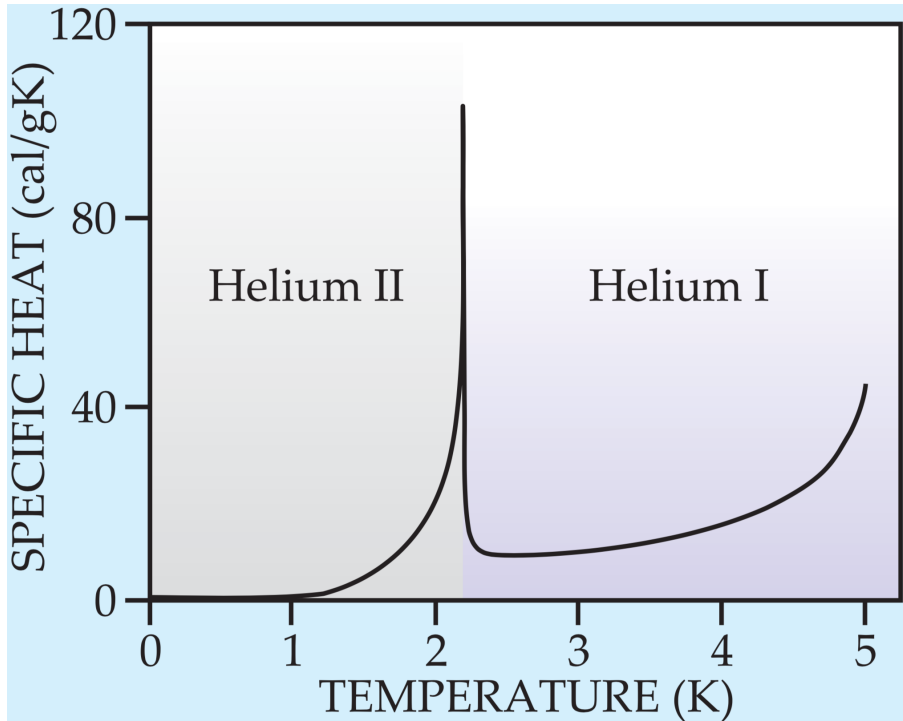


Figure 1.1: The specific heat of ^4He as a function of the temperature. There is a clearly visible singularity around 2.2 K and the graph itself has the distinct λ -like shape that inspired^[9] Willem and Anna Keesom to call the temperature at which the singularity occurs the “ λ -point”. (Illustration courtesy of R.J. Donnelly^[10])

The year after, in 1936, Willem and Anna Keesom measured an abnormally high heat conductance below T_λ ^[3]. This was confirmed roughly one year later by J.F. Allen *et al.*^[18] and it was understood that the high thermal conductance was the reason for the helium to stop boiling whenever the temperature drops below T_λ . It was in 1937, when Kapitza tried to determine the viscosity of the laminar flow, that he measured a viscosity that was about 10^4 times smaller than that of hydrogen gas^[1]. It was then that Kapitza, by analogy with superconductors, first coined the word “superfluid”^[1] to describe the special state that helium enters below the λ -point where it can flow, seemingly without friction. Allen and Misener realised that superfluid helium is not just a liquid with a very low viscosity, but that its hydrodynamics was completely different from that of ordinary liquids^[19] and therefore required a completely new interpretation.

A beginning to this new interpretation was made by London^[20] in 1938 when he made a connection between the behaviour of superfluid helium and that of an ideal “Bose-Einstein” (BE) gas. Both his calculated value for $T_c = 3.09\text{ K}$ and the behaviour of the temperature dependence of the heat capacity for the ideal BE-gas were very similar to the measured ones for liquid helium below T_λ . He wrote to Nature that “it was difficult not to imagine a connection with “Bose-Einstein condensation” (BEC). Tisza expanded upon London’s ideas^[21] and considered a Helium II system of total N atoms to consist of two parts; a macroscopic “condensed” part n_0 , the superfluid component, in the ground state, and the remaining part $n = N - n_0$, the normal component, where the helium atoms are distributed over the excited states. Assuming this was correct the

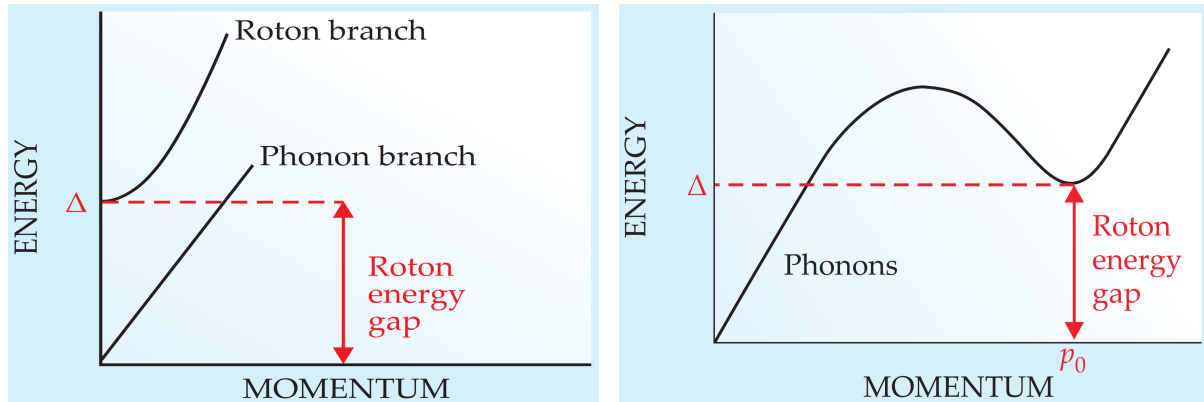


Figure 1.2: Left: Lev Landau’s 1941 energy dispersion curve^[22] for the excitations in liquid helium below T_λ . It exhibits a phonon- and a roton branch. The slope of the linear phonon branch corresponds to the velocity of sound. Right: Lev Landau’s 1947 modified dispersion curve. The roton-branch is no longer a separate excitation branch but rather an extension of the phonon-branch. (Illustration courtesy of R.J. Donnelly^[10])

fraction n_0/N should decrease with increasing temperature according to the equation

$$\frac{n_0}{N} = 1 - \left(\frac{T}{T_0} \right)^s \quad \text{for } T < T_0 \quad (1.1)$$

where $s = 3/2$ for an ideal gas and should be taken larger, e.g. $s = 5$, for a real liquid with stronger interactions between the atoms.

This was the birth of the “two-fluid” model. Within the framework of this model he derived two hydrodynamic equations for liquid helium below T_λ and concluded that within superfluid liquid helium, heat propagates in waves instead of diffusing through the medium, and calculated the velocity of these waves. He also explained why the viscosity is disappearing at low temperatures contrary to classical liquids where the viscosity increases^[4–7]. In 1941 Lev Landau reformulated Tisza’s theory on a more rigorous footing^[22,23]. He assumed, contrary to Tisza, that the normal component of the liquid was made-up of collective excitations instead of excited single atoms. He postulated that the liquid could exhibit two states of motion which he called “potential motion” that is irrotational ($\nabla \times \mathbf{v} = 0$), and “vortex motion” that is rotational ($\nabla \times \mathbf{v} \neq 0$). The corresponding energies of these two motions are separated by an energy gap Δ . In case of potential internal motion the excitations are quanta of longitudinal (sound) waves, i.e., phonons. The excitations of the vortex-spectrum could be called “rotons” (see Figure 1.2).

A theoretical demonstration, explicitly showing that phonons and rotons are collective excitations of the liquid, came in the form of a 1947 paper by Nikolay Bogolyubov^[24]. The intimate relationship between superfluidity and BEC was not universally accepted until 1995 when Cornell and Wieman in Colorado and Ketterle at MIT discovered BEC in rubidium quantum gases^[25,26].

1.2 SOME KEY CONCEPTS

In this section I briefly introduce some key ideas that are used throughout the thesis and that are needed to fully appreciate the discussed material. Most of this introduction is guided by the work of Pitaevskii and Stringari^[27] on Bose-Einstein condensation. Also references to more complete and more in-depth treatments are provided for the interested reader.

1.2.1 BOSE-EINSTEIN CONDENSATION AND LONG-RANGE ORDER

The essential concept of Bose-Einstein (BE) condensation is the fact that at low temperatures, multiple bosons, unlike fermions, occupy the same quantum state. In theory there is no upper bound on how many bosons can occupy such a single state. It is then said that, with ever decreasing temperature, a macroscopic part of the total number of bosons will “condense” into the quantum state with the lowest energy.

Another important concept in BEC is the idea of long-range order. Let us start by introducing the one-body density matrix of a system of N bosons in a pure state $\Psi_k(\mathbf{r}_1, \mathbf{r}_2, \dots, \mathbf{r}_N)$

$$n_k^{(1)}(\mathbf{r}, \mathbf{r}') := N \int \Psi_k^*(\mathbf{r}, \mathbf{r}_2, \dots, \mathbf{r}_N) \Psi_k(\mathbf{r}', \mathbf{r}_2, \dots, \mathbf{r}_N) d\mathbf{r}_2 d\mathbf{r}_3 \dots d\mathbf{r}_N \quad (1.2)$$

where the integral is taken over the $N - 1$ coordinates $\mathbf{r}_2, \mathbf{r}_3, \dots, \mathbf{r}_N$. For a statistical mixture of quantum states one needs to take the weighted average over all the different Ψ_k -states. At thermodynamic equilibrium the states are Boltzmann weighted by their eigenvalues $\{E_k\}$

$$n^{(1)}(\mathbf{r}, \mathbf{r}') = \frac{1}{Q} \sum_k n_k^{(1)}(\mathbf{r}, \mathbf{r}') e^{-E_k/k_B T} \quad (1.3)$$

where Q is the partition function. For more general cases the one-body density matrix is defined

$$n^{(1)}(\mathbf{r}, \mathbf{r}') := \langle \hat{\Psi}^\dagger(\mathbf{r}) \hat{\Psi}(\mathbf{r}') \rangle \quad (1.4)$$

where $\hat{\Psi}^\dagger(\mathbf{r})/\hat{\Psi}(\mathbf{r})$ are field-operators creating/annihilating a boson at \mathbf{r} and the averaging $\langle \dots \rangle$ is taken over all states in the mixture. Once it is accepted that a macroscopic part of the total number of bosons can occupy a single quantum state it can be demonstrated that, while considering a uniform isotropic system of N bosons, the one-body density matrix (Equation (1.2)) tends to a constant value when the distance between \mathbf{r} and \mathbf{r}' goes to infinity. In the thermodynamic limit where $N, V \rightarrow \infty$ such that $n = N/V$ is kept fixed, the one-body density only depends on the modulus of the relative variable $\mathbf{s} := \mathbf{r} - \mathbf{r}'$ so that we can write it as the Fourier transform of the momentum distribution as

$$n^{(1)}(s) = \frac{1}{V} \int n^{(1)}(\mathbf{p}) \exp(i\mathbf{p} \cdot \mathbf{s}/\hbar) d\mathbf{p} \quad (1.5)$$

For a BEC system, the momentum distribution at small momenta is not smooth but has a sharp peak around $p = 0$ for the bosons that are in the ground state, while the remaining bosons are smoothly distributed over the excited states.

$$n(\mathbf{p}) = N_0 \delta(\mathbf{p}) + \tilde{n}(\mathbf{p}) \quad (1.6)$$

where \tilde{n} is a smoothly varying function of \mathbf{p} . When this expression is plugged into Equation (1.5) and taking the limit where s goes to infinity it is obtained that

$$\lim_{s \rightarrow \infty} n^{(1)}(s) = \frac{N_0}{V}, \quad (1.7)$$

where $N_0/V := n_0 \leq 1$ is called the condensate fraction. It is called long-range order since it involves the off-diagonal elements of the one-body density matrix; the elements that are usually associated with the coherences.

A set of eigenvalues $\{n_i\}$ of the one-body density matrix can be defined through the following eigenvalue equation

$$\int n^{(1)}(\mathbf{r}, \mathbf{r}') \varphi_i(\mathbf{r}') d\mathbf{r}' = n_i \varphi_i(\mathbf{r}) \quad (1.8)$$

and its solutions $\{\varphi_i\}$ form a natural orthonormal basis set of single boson wave functions $\int \varphi_i^* \varphi_j d\mathbf{r} = \delta_{ij}$, with normalisation condition $\sum_i n_i = N$. This permits writing the one-body density matrix in a useful diagonalised form. Recalling that BEC occurs when a single particle state φ_i is occupied in a macroscopic way, say when $n_{i=0} = N_0$, a number of order N , we separate the condensate part from the rest

$$n^{(1)}(\mathbf{r}, \mathbf{r}') = N_0 \varphi_0^*(\mathbf{r}) \varphi_0(\mathbf{r}') + \sum_{i \neq 0} n_i \varphi_i^*(\mathbf{r}) \varphi_i(\mathbf{r}') \quad (1.9)$$

1.2.2 BOGOLYUBOV'S APPROXIMATION AND THE ORDER PARAMETER

It is customary, given the importance of the condensate fraction N_0 in a BEC, to write the field operator of a N -body boson system as the sum of the condensate part and the rest, just as the one-body density matrix

$$\hat{\Psi}(\mathbf{r}) = \varphi_0(\mathbf{r}) \hat{a}_0 + \sum_{i \neq 0} \varphi_i(\mathbf{r}) \hat{a}_i \quad (1.10)$$

where \hat{a}_i and \hat{a}_i^\dagger are the annihilation and creation operator of a particle in state φ_i and obey the usual bosonic commutation relations

$$[\hat{a}_i, \hat{a}_j^\dagger] = \delta_{ij}, \quad [\hat{a}_i, \hat{a}_j] = 0 = [\hat{a}_i^\dagger, \hat{a}_j^\dagger] \quad (1.11)$$

Using Equation (1.10) in Equation (1.2) and comparing it to Equation (1.9) one finds the expectation value of $\langle \hat{a}_j^\dagger \hat{a}_i \rangle = \delta_{ij} n_i$. Now, the Bogolyubov approximation essentially

replaces the operators \hat{a}_0 and \hat{a}_0^\dagger with the *c*-number¹ $\sqrt{N_0}$. This is equivalent to ignoring the non-commutative nature of the operators due to the macroscopic occupation of the state φ_0 , when $N_0 = \langle \hat{a}_0^\dagger \hat{a}_0 \rangle \gg 1$. We then rewrite the field operator as the sum of a classical field for the condensed component and a quantum field for the non-condensed component

$$\hat{\Psi}(\mathbf{r}) = \Psi_0(\mathbf{r}) + \delta\hat{\Psi}(\mathbf{r}), \quad (1.12)$$

where $\delta\hat{\Psi}(\mathbf{r}) = \sum_{i \neq 0} \varphi_i(\mathbf{r}) \hat{a}_i$ and $\Psi_0(\mathbf{r}) = \sqrt{N_0} \varphi_0(\mathbf{r})$. At $T = 0$ the whole system is condensed and one can ignore $\delta\hat{\Psi}$ altogether; the field operator becomes a normal function of space Ψ_0 .

The classical field Ψ_0 is called the *effective-* or *macroscopic* wave function of the condensate. It behaves like an order parameter in the sense that it represents the phase transition between the normal liquid phase and the superfluid phase. It varies continuously between the maximum value \sqrt{N} , which is proportional to the total number of bosons in the condensate at $T = 0$, and vanishes at the superfluid/normal liquid phase transition temperature T_λ . It is a complex quantity characterised by a real-valued modulus and phase:

$$\Psi_0(\mathbf{r}) = \left| \sqrt{N_0} \varphi_0(\mathbf{r}) \right| e^{iS(\mathbf{r})} \quad (1.13)$$

The modulus determines the number-density of the condensate, while the phase S plays an important role in the coherence and properties of the superfluid. As we will see in Section 1.2.4, S plays the role of a velocity potential.

Using an order parameter as defined here is equivalent to using the many-body wave function

$$\Phi(\mathbf{r}_1, \mathbf{r}_2, \dots, \mathbf{r}_N) = \prod_{i=1}^N \varphi_0(\mathbf{r}_i), \quad (1.14)$$

with a density operator $\hat{\rho}(\mathbf{r}) := \sum_{i=1}^N \delta(\mathbf{r} - \mathbf{r}_i)$ (see Section 2.1). One way to see why this wave function plays the role of an order parameter is to look at its time dependence. For normal wave functions the time dependence is determined by the eigenvalues E_i of the Hamiltonian of the system

$$\Psi(\mathbf{r}, t) = \psi(\mathbf{r}) e^{-iE_i t/\hbar} \quad (1.15)$$

But in this case, the time dependence is determined by the chemical potential $\mu = E(N) - E(N-1) \approx \partial E / \partial N$

$$\Psi_0(\mathbf{r}, t) = \Psi_0(\mathbf{r}) e^{-i\mu t/\hbar} \quad (1.16)$$

Another aspect of Ψ_0 being an order parameter and not a true many-body wave function is that two solutions Ψ_a and Ψ_b of the non-linear droplet Hamiltonian corresponding to two different values of the chemical potential μ_a and μ_b are not necessarily orthogonal, i.e. $0 \leq N^{-1} \int \Psi_a^* \Psi_b \, d\mathbf{r} < 1$.

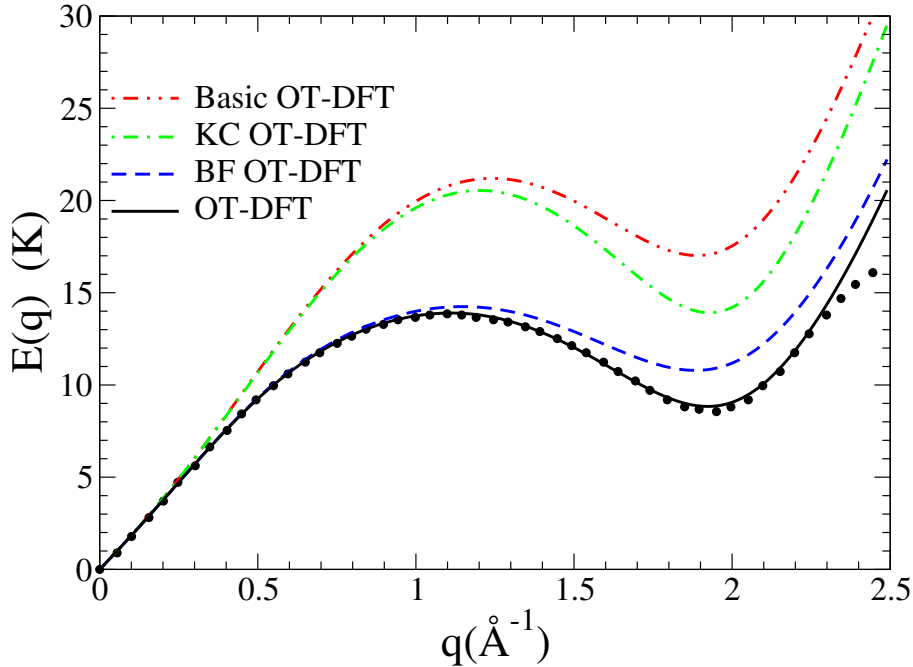


Figure 1.3: Dispersion relation for elementary excitations in liquid ^4He calculated as in^[28]. ‘Basic’ indicates the Orsay-Trento (OT) functional^[29] without the non-local kinetic energy correction (KC) nor the back-flow (BF) terms; KC OT-DFT adds to the basic OT-DFT the KC term; BF OT-DFT adds to the basic OT-DFT the BF term. The dots are the experimental data from^[30]. The Landau velocity $v_L = E(q)/(\hbar q)|_{min}$ obtained for each functional is 60.3 m/s (OT-DFT); 75.1 m/s (BF OT-DFT); 94.4 m/s (KC OT-DFT); 118 m/s (basic OT-DFT); and 57.5 m/s (experiment). See also Section 2.2.

1.2.3 LANDAU’S CRITERION FOR SUPERFLUIDITY

For a gas or liquid to be able to become superfluid Landau postulated that the energy dispersion relation needs to fulfil certain requirements. Specifically for a fluid to flow without dissipation, i.e. a super-flow, the velocity field needs to fulfil the following inequality:

$$v < v_c = \min_{\mathbf{p}} \frac{\epsilon(\mathbf{p})}{p} \quad (1.17)$$

For an ideal Bose gas $\epsilon(\mathbf{p}) = \frac{p^2}{2m}$. In this case

$$v_c = \min_{\mathbf{p}} \frac{\epsilon(\mathbf{p})}{p} \quad (1.18)$$

$$= \min_{\mathbf{p}} \frac{p}{2m} \quad (1.19)$$

$$= 0 \quad (1.20)$$

Apparently an ideal Bose-gas cannot become superfluid.

¹The term *c*-number is old nomenclature for a classical number, which can be real or complex, to distinguish them from quantum numbers, or *q*-numbers, that are represented by operators.

But if we allow for some weak interactions between the bosons the energy dispersion relation is given by

$$\epsilon(\mathbf{p}) = \sqrt{\frac{gn}{m}p^2 + \left(\frac{p^2}{2m}\right)^2}, \quad (1.21)$$

Bogolyubov's dispersion law for elementary excitations (1947). And thus

$$v_c = \min_{\mathbf{p}} \sqrt{\frac{gn}{m} + \frac{p^2}{4m^2}} \quad (1.22)$$

$$= \sqrt{\frac{gn}{m}} \quad (1.23)$$

$$= c, \quad (1.24)$$

the speed of sound. Here $g = \frac{4\pi\hbar^2 a}{m}$, and a the s -wave scattering length. The weakly interacting Bose gases can become superfluid.

Liquid helium below the λ -point has a similar energy dispersion relation (see Figure 1.3) hence reinforcing the notion that superfluidity and Bose-Einstein condensation are two intimately related concepts. The experimental value of the speed of sound in bulk superfluid liquid helium is ~ 57.5 m/s.

1.2.4 ROTATION AND VORTICITY IN SUPERFLUIDS

We introduce here the concept of quantised vortices in the DFT approach. It will be shown later in Section 2.1.1 that within the DFT framework, the order parameter Ψ is a solution of the time-dependent Euler-Lagrange (EL) Equation (2.13). Taking this for granted for now, lets start with Equation (2.13) and the order parameter from Equation (1.13), dropping the ground-state subscript and allowing φ and S to vary in time

$$i\hbar \frac{\partial}{\partial t} \Psi(\mathbf{r}, t) = \left[-\frac{\hbar^2}{2m} \nabla^2 + \frac{\delta \mathcal{E}_c}{\delta \rho} \right] \Psi(\mathbf{r}, t) \quad (1.25)$$

one left-multiplies it with the complex conjugate of the order parameter Ψ^* and then subtract the complex conjugate of the whole expression on both sides. After some algebra and defining $\rho(\mathbf{r}, t) := N|\varphi(\mathbf{r}, t)|^2$, one arrives at the continuity equation

$$\frac{\partial \rho}{\partial t} + \nabla \cdot \mathbf{j} = 0, \quad (1.26)$$

with

$$\mathbf{j}(\mathbf{r}, t) := -\frac{i\hbar}{2m} [\Psi^*(\mathbf{r}, t) \nabla \Psi(\mathbf{r}, t) - \Psi(\mathbf{r}, t) \nabla \Psi^*(\mathbf{r}, t)] \quad (1.27)$$

$$= \rho(\mathbf{r}, t) \frac{\hbar}{m} \nabla S(\mathbf{r}, t) \quad (1.28)$$

From Equation (1.26) it follows that the atomic number density is a conserved quantity.

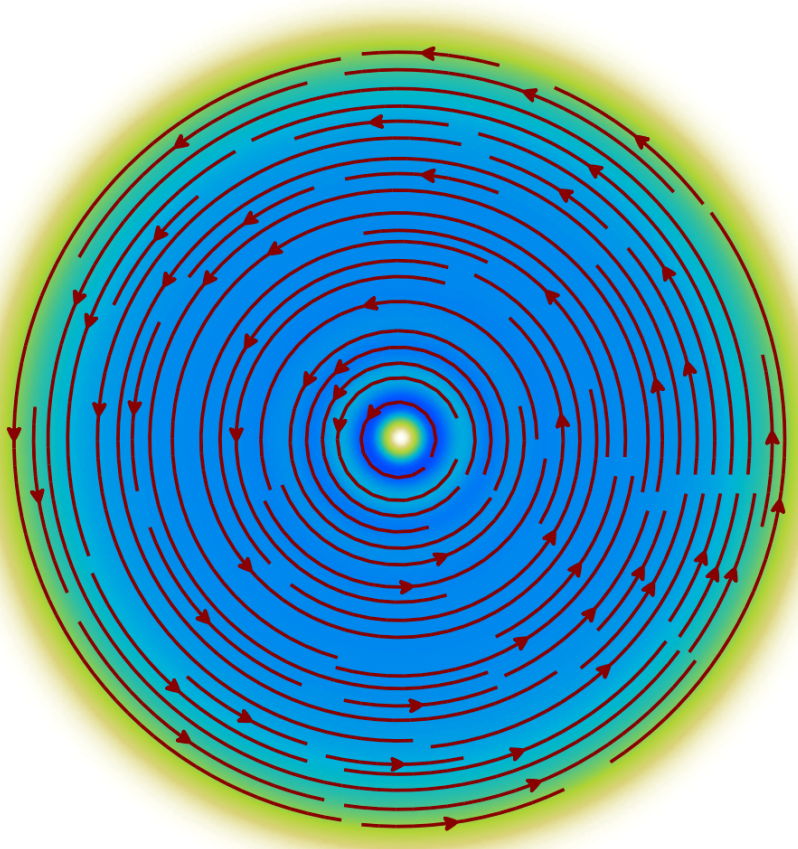


Figure 1.4: Cross section of a ${}^4\text{He}$ droplet through a symmetry plane. The droplet is made of 1000 atoms. Superimposed are the streamlines of the velocity field \mathbf{v}_s for $s = 1$. They are concentric circles, centred around the vortex core along the z -axis. The colour scale represents the the number density $\rho(r)$ where bluer means a higher value. The radius of the droplet is about 22 Å.

We can identify the collective velocity \mathbf{v}_s of the superfluid through the relation

$$\mathbf{v}_s(\mathbf{r}, t) = \mathbf{j}/\rho = \frac{\hbar}{m} \nabla S(\mathbf{r}, t) \quad (1.29)$$

and we see that the rotation of the velocity field of the superfluid $\nabla \times \mathbf{v}_s = 0$, i.e. the fluid is said to be *irrotational*; a typical property of superfluids. Conversely, taking the curl $\nabla \times \mathbf{j} = \frac{\hbar}{m} \nabla \rho \times \nabla S$ we see that this is merely a restatement of the fact that one needs a gas or liquid with a non-uniform density and a non-zero phase for it to be able to support vortices.

Let us consider the illustrative example of a line vortex through the origin along the z -axis. As will be demonstrated in Section 2.3.1, this is a stationary state of the droplet Hamiltonian and therefore its time dependence is just a multiplicative factor. In cylindrical coordinates (r, φ, z) such a vortex solution has the form

$$\Psi_s(\mathbf{r}) = \sqrt{\rho(r)} e^{is\varphi}, \quad (1.30)$$

with s , the angular momentum, an integer. This is an eigenfunction of the angular

momentum operator \hat{L}_z with eigenvalue

$$\hat{L}_z \Psi_s(\mathbf{r}) = \frac{\hbar}{i} \frac{\partial}{\partial \varphi} \Psi_s(\mathbf{r}) = \hbar s \Psi_s(\mathbf{r}) \quad (1.31)$$

and with expectation value

$$\langle \hat{L}_z \rangle = \langle \Psi_s | \hat{L}_z | \Psi_s \rangle \quad (1.32)$$

$$= \hbar s \left\langle \sqrt{N_0} \varphi_0 \middle| \sqrt{N_0} \varphi_0 \right\rangle \quad (1.33)$$

$$= N_0 \hbar s \quad (1.34)$$

The angular momentum is quantised in units of \hbar and proportional to the number of bosons in the BEC fraction/superfluid. We can calculate the velocity field

$$\mathbf{v}_s = \frac{\hbar}{m} \nabla S = \frac{\hbar s}{m r} \hat{\varphi} \quad (1.35)$$

The streamlines of \mathbf{v}_s are concentric circles, centred around the z -axis, lying in the xy -plane (see Figure 1.4). Contrary to rigid rotation fields which increase proportional to the distance from the z -axis r , the superfluid rotation field decreases proportional to the inverse of the distance from the z -axis $1/r$ and is singular in the origin. Calculating the circulation of the velocity field \mathbf{v}_s along a closed contour including the z -axis gives

$$\oint_{\partial\Sigma} \mathbf{v}_s \cdot d\mathbf{l} = \int_0^{2\pi} \frac{\hbar s}{m r} \hat{\varphi} \cdot r d\varphi \hat{\varphi} \quad (1.36)$$

$$= s \frac{\hbar}{m} \quad (1.37)$$

where $h = 2\pi\hbar$ is Planck's constant. There are two things to note here. Firstly, the circulation around a closed loop that encompasses the z -axis is quantised in units of h/m for $s \in \mathbb{N}_{>0}$. Secondly, the value of the circulation of the velocity field does not depend on the chosen contour as long as it includes the location of the vortex. This means that all the vorticity is contained at the location where the velocity field is singular (the "core" of the vortex), at $r = 0$ along the z -axis.

Because of the pole in the velocity field, Stokes' theorem will lead to the following contradiction

$$s \frac{\hbar}{m} = \oint_{\partial\Sigma} \mathbf{v}_s \cdot d\mathbf{l} = \iint_{\Sigma} \nabla \times \mathbf{v}_s \cdot d\Sigma = 0 \quad (1.38)$$

and can therefore not be applied. To emphasise that all the vorticity is concentrated around the vortex core one can write formally

$$\nabla \times \mathbf{v}_s = s \frac{\hbar}{m} \delta^{(2)}(\mathbf{r}_\perp) \hat{\mathbf{z}}, \quad (1.39)$$

where $\delta^{(2)}$ is 2-dimensional Dirac-delta function and \mathbf{r}_\perp a vector in a plane perpendicular to the vortex line.

1.3 HELIUM DROPLETS

Until the 1980's, most experimental and theoretical work was done on bulk systems, i.e. systems of the order of N_A number of atoms. It was only in the last couple of decades that advancements in technology enabled experimentalists to create nanoscale sized superfluid helium droplets. From the early 1990's onwards, superfluid helium nano-droplets became an active field of study, both experimentally and theoretically.

Helium nanodroplets are considered ideal model systems to explore quantum hydrodynamics in self-contained, isolated superfluids. The main focus has been on the evolution of their properties with the number of atoms in the cluster, until the condensed matter limit is reached. Helium clusters are especially interesting in that quantum effects play a key role in determining their properties. In particular, given that a helium cluster is an ensemble of bosons at about 0.4 K^[31,32], manifestations of collective behaviour (such as superfluidity) are expected. On the other hand, it is not yet clear how the finite size of a cluster affects this non-classical (or degenerate) collective behaviour.

Recently, Toennies et al.^[33] have measured the electronic spectrum of glyoxal molecules embedded in He clusters and found it consistent with a theoretical simulation computed using the phonon dispersion curve of superfluid bulk He II. The authors themselves, however, point out that at the average cluster size of 5500 He atoms reported in Ref. [33], the clusters are so big that finite size effects in the interior region are negligible (see also Refs. [34, 35]). It is therefore not surprising that they find results consistent with the bulk case, especially for a molecule readily solvated inside the cluster, for which surface effects play a minor role. Therefore the influence of the He clusters size on superfluidity has not been detected so far.

The helium-helium interaction is already weak in bulk liquid helium and in finite self-bound systems such as droplets it is even weaker, e.g. the binding energy per atom is < 7.17 K. Because of this helium droplets cool down very rapidly due to fast evaporation and therefore reaching their limiting temperature of about 0.38 K in microseconds. Pure helium droplets are neutral systems and their properties like their size, binding energy and excitation spectra, are not easy to determine experimentally and are usually obtained by indirect methods. This did not stop the theoreticians describe doped ${}^4\text{He}_N$ droplets using a wide variety of approaches depending on the size and character of the droplets ranging from Quantum Monte Carlo, Hypernetted-Chain/Euler-Lagrange^[36], Variational Monte Carlo and many others.

A key property of helium droplets, in contrast to bulk helium, is their ability to pickup any kind of dopants with which they collide. Depending on the strength of the dopant- ${}^4\text{He}$ interaction and the surface tension of the droplet, a dimensionless parameter λ can be defined^[37] with a critical value $\lambda_0 \sim 1.9$. Below λ_0 impurities are bound to the surface of the droplet (e.g. the alkalis), and above they get solvated into the droplet's interior. Droplets can therefore be doped with almost any kind of atomic- or molecular species.

From the perspective of the droplet it this means that it is possible to use the dopants as gentle probes to determine the superfluid properties of helium droplets that would be inaccessible with other methods. For two examples of this see Refs. [38–40], where a

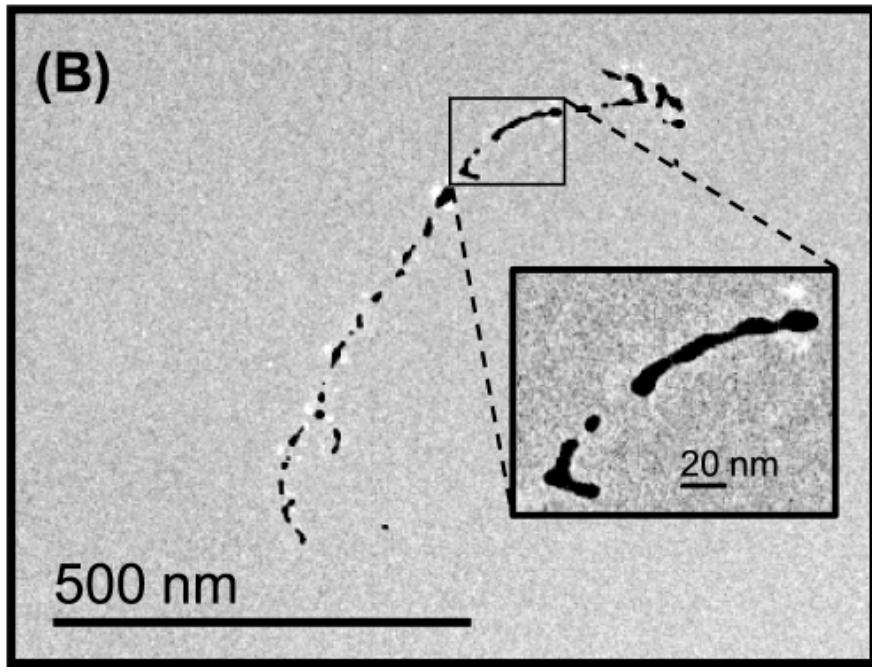


Figure 1.5: Electron-microscope image of an elongated track-shaped Ag-cluster after it is surface-deposited.

dopant is used to probe the superfluid character of small ^4He droplets and Refs. [41, 42] to see their limiting temperatures.

Moreover, from the perspective of the impurities it enables a broad spectrum of possible experimental studies. Due to the fact that helium droplets are ultra cold superfluid liquids, and therefore provide high mobility of any picked-up dopants, one can conduct high resolution spectroscopy studies. Having a fine control over the number of picked-up dopants[29] one can use droplets as a matrix for creating self-organising structures of polar molecules, or very cold metal clusters and study their Coulomb explosion.

One of the most intriguing properties of superfluid helium droplets is the fact that they can host quantised vortices. Because of their ultra low temperature they are true quantum liquids and their vorticity and angular momentum are quantised. The existence of quantised vortices was anticipated because they have been created and observed in BECs made of dilute gases. However, the detection of quantised vortices is still experimentally challenging (see Section 4 in this thesis).

A lot of work has been done on helium droplets the last few decades, both experimentally and theoretically. From the absorption spectra of alkali metal doped helium droplets, the study of doped mixed ^3He - ^4He droplets, electrons in liquid helium, to the investigation of the critical Landau velocity inside small ^4He droplet. For a comprehensive overview of work done in the last two decades, the interested reader is referred to the review papers in Refs. [43–45].

2

THE DFT METHOD FOR HEAVY IMPURITIES

One Functional to rule them all,
One Functional to find them,
One Functional to bring them all and
in a droplet bind them.

F.M.G.J. Coppens

FROM a theoretical point of view, superfluid helium must be considered as a high dimensional quantum system. Quantum Monte Carlo (QMC)^[46] and direct quantum mechanical^[47–49] calculations are the most accurate methods, but their computational demand quickly exceeds currently available computer resources when the number of helium atoms increases. Furthermore, QMC cannot describe dynamic evolution of superfluid helium in real time. To address these limitations, semi-empirical methods based on density functional theory (DFT) formalism have been introduced^[50–52]. DFT can be applied to much larger systems than QMC and allows for time-dependent formulation. As such, it offers a good compromise between accuracy and computational feasibility. The main drawback of DFT is that the exact energy functional is not known and must therefore be constructed in a semi-empirical manner. Moreover, doped helium droplets are limited to a mean-field description of the dopant-helium interaction. Nevertheless, DFT is the only method to date that can successfully reproduce results from a wide range of time-resolved experiments in superfluid helium, for realistic sizes compared to experimental conditions.

2.1 THE KOHN-SHAM APPROACH

The starting point for the density functional method is the Hohenberg-Kohn (HK) theorem^[53], which states that the ground-state energy E_v of an *interacting inhomogeneous* system in a static potential v can be written in as a unique functional of the one-body

density ρ like

$$E_v[\rho] = \int v(\mathbf{r})\rho(\mathbf{r}) d\mathbf{r} + F[\rho] \quad (2.1)$$

where $F[\rho]$ is a universal functional—valid for *any* number of particles and *any* external potential v —of the one-body density, defined as

$$\rho(\mathbf{r}) := \langle \Phi | \hat{\rho}(\mathbf{r}) | \Phi \rangle = \left\langle \Phi \left| \sum_{i=1}^N \delta(\mathbf{r} - \mathbf{r}_i) \right| \Phi \right\rangle \quad (2.2)$$

and $\Phi(\mathbf{r}_1, \mathbf{r}_2, \dots, \mathbf{r}_N)$ is the many-body wave function of such a system. Furthermore, the functional $F[\rho]$ gives the ground state energy *if and only if* the input density is the true ground state density of the system.

Kohn and Sham (KS) later reformulated^[54] the theory by introducing an approximation scheme for the functional $F[\rho]$ that is analogues to Hartree's method, but also contains the major part of the correlation effects inherent in interacting many-body systems. The approximation starts by defining

$$F[\rho] := T[\rho] + E_c[\rho] \quad (2.3)$$

where $T[\rho]$ is now the kinetic energy of a fictitious system of *non-interacting* particles with density ρ and $E_c[\rho]$ is the correlation energy of an *interacting* system with the same density. For the kinetic part this allows us two write the total kinetic energy $T[\rho]$ as the sum over the individual kinetic energies T_i of the non-interacting particles

$$T = \sum_i T_i = -\frac{\hbar^2}{2m} \sum_i \langle \varphi_i | \nabla^2 | \varphi_i \rangle = -\frac{\hbar^2}{2m} \sum_i \int \varphi_i^*(\mathbf{r}) \nabla^2 \varphi_i(\mathbf{r}) d\mathbf{r}, \quad (2.4)$$

where the $\{\varphi_i\}$ are the Kohn-Sham single-particle orbitals corresponding to the many-body KS wave function $\Phi_{KS}(\mathbf{r}_1, \mathbf{r}_2, \dots, \mathbf{r}_N) = \prod_i \varphi_i(\mathbf{r}_i)$ and leading to the density (using the definition in Equation (2.2)) $\rho(\mathbf{r}) = \sum_i |\varphi_i(\mathbf{r})|^2$.

There is difference between the true kinetic energy of the interacting system and the fictitious one, due to the negligence of the correlations. This difference is being corrected and accounted for in the correlation energy $E_c[\rho]$.

Because the functional we used in this work is calibrated to produce the correct behaviour of bulk liquid helium at zero temperature $T = 0$ and zero pressure $P = 0$, we assume complete Bose-Einstein (BE) condensation of the helium. In this case all the helium atoms occupy the same single-particle KS-orbital φ_0 . Therefore the many-body wave function and the density simplifies further to

$$\Phi_{BEC}(\mathbf{r}_1, \mathbf{r}_2, \dots, \mathbf{r}_N) = \prod_i \varphi_0(\mathbf{r}_i) \quad (2.5)$$

and

$$\rho(\mathbf{r}) = N |\varphi_0(\mathbf{r})|^2 \quad (2.6)$$

respectively. As explained in Section 1.2.2, it is customary to define an effective wave function

$$\Psi(\mathbf{r}) := \sqrt{\rho(\mathbf{r})} = \sqrt{N}\varphi_0(\mathbf{r}) \quad (2.7)$$

for the condensate (see Equation (1.12)), which is sometimes called a *macroscopic wave function* or *order parameter*. We can now simplify the expression for the kinetic energy (Equation (2.4))

$$T = -\frac{\hbar^2}{2m} N \int \varphi_0^*(\mathbf{r}) \nabla^2 \varphi_0(\mathbf{r}) d\mathbf{r} = \frac{\hbar^2}{2m} N \int |\nabla \varphi_0|^2 d\mathbf{r}, \quad (2.8)$$

where we used partial integration to get to the last step and imposed that the orbital φ_0 vanishes at the boundaries. With our definition Equation (2.7) we can now write the kinetic energy as a functional of the density

$$T[\rho] = \frac{\hbar^2}{2m} \int |\nabla \sqrt{\rho}|^2 d\mathbf{r} \quad (2.9)$$

To summarise, we write the complete energy functional E_v as

$$E_v[\rho] = \int v(\mathbf{r}) \rho(\mathbf{r}) d\mathbf{r} + \frac{\hbar^2}{2m} \int |\nabla \sqrt{\rho}|^2 d\mathbf{r} + \int \mathcal{E}_c[\rho] d\mathbf{r} \quad (2.10)$$

where we defined the correlation energy density functional \mathcal{E}_c through

$$\mathcal{E}_c[\rho] := \int \mathcal{E}_c[\rho] d\mathbf{r}. \quad (2.11)$$

The job now is to find an \mathcal{E}_c such that the desired physical properties of helium can be recovered. This is far from trivial but several of these density functionals are available now. The one used in this work is discussed in Section 2.2.

2.1.1 TIME-DEPENDENT DFT

To describe the time evolution of the system, the Runge-Gross theorem extends DFT to its time-dependent version TDDFT^[55]. The functional variation of the associated action (see Equation (2.48) for an example) leads to the following time-dependent Euler-Lagrange (EL) equation

$$i\hbar \frac{\partial}{\partial t} \Psi(\mathbf{r}, t) = \left\{ -\frac{\hbar^2}{2m} \nabla^2 + \frac{\delta \mathcal{E}_c}{\delta \rho} \right\} \Psi(\mathbf{r}, t) := \mathcal{H}[\rho] \Psi(\mathbf{r}, t) \quad (2.12)$$

As long as we are in the thermodynamic regime the solutions $\Psi(\mathbf{r}, t)$ can be decomposed into the liquid density and associated velocity potential field (see Section 1.2.2 and Section 1.2.4).

Considering only eigenstates $\Psi(\mathbf{r}, t) = \Psi_0(\mathbf{r}) e^{-i\mu t/\hbar}$ of the time independent Hamiltonian $\mathcal{H}[\rho]$ the time-dependent EL-equation reduces to a time independent one

$$\left\{ -\frac{\hbar^2}{2m} \nabla^2 + \frac{\delta \mathcal{E}_c}{\delta \rho} \right\} \Psi_0(\mathbf{r}) = \mu \Psi_0(\mathbf{r}) \quad (2.13)$$

Table 2.1: Model parameters for the OT-DFT and solid functionals.

ϵ_{LJ} (K)	σ (\AA)	h (\AA)	c_2 (K \AA ⁶)	c_3 (K \AA ⁹)	α_s (\AA ³)
10.22	2.556	2.190323	-2.41186×10^4	1.85850×10^6	54.31
ρ_{0s} (\AA ⁻³)	l (\AA)	C (Hartree)	β (\AA ³)	ρ_m (\AA ⁻³)	γ_{11}
0.04	1.	0.1	40.	0.37	-19.7544
γ_{12} (\AA ⁻²)	α_1 (\AA ⁻²)	γ_{21}	γ_{22} (\AA ⁻²)	α_2 (\AA ⁻²)	
12.5616	1.023	-0.2395	0.0312	0.14912	

with μ the chemical potential. Solving this equation by iteration will result in the ground state density $|\Psi_0|^2$ of the system. Within the HK-framework and the variation principle that was used to obtain these EL-equations, the nature of the minimisation is such that it gives the lowest energy for a given symmetry. This means that as long as the input state does not break the symmetry of the time-independent EL-equation, it minimises the energy of this state even if it does not lead to the ground state. This can be used to obtain a stationary vortex-line solution. With the inclusion of appropriate constraints in the energy functional the same procedure can be used to obtain helium densities with an array of vortex-lines.

2.2 THE ORSAY-TRENTO DENSITY FUNCTIONAL

The functional that is used in the work presented in this thesis is based on the Orsay-Trento (OT) functional^[29]. It uses a finite-range, non-local approach and it is, to date the most accurate model in the sense that its parameters were fitted to reproduce the bulk properties of liquid helium at $T = 0 = P$. It is

$$\begin{aligned} \mathcal{E}_c[\rho, \mathbf{v}] = & \frac{1}{2} \int \left\{ \rho(\mathbf{r}) V_{LJ}(|\mathbf{r} - \mathbf{r}'|) \rho(\mathbf{r}') \right. \\ & + \frac{1}{2} c_2 \rho(\mathbf{r}) [\bar{\rho}(\mathbf{r})]^2 + \frac{1}{3} c_3 \rho(\mathbf{r}) [\bar{\rho}(\mathbf{r})]^3 \Big\} d\mathbf{r}' \\ & - \frac{\hbar^2}{4m} \alpha_s \int F(|\mathbf{r} - \mathbf{r}'|) \left[1 - \frac{\tilde{\rho}(\mathbf{r})}{\rho_{0s}} \right] \nabla \rho(\mathbf{r}) \cdot \nabla \rho(\mathbf{r}') \left[1 - \frac{\tilde{\rho}(\mathbf{r}')}{\rho_{0s}} \right] d\mathbf{r}' \\ & - \frac{m}{4} \int V_J(|\mathbf{r} - \mathbf{r}'|) \rho(\mathbf{r}) \rho(\mathbf{r}') [\mathbf{v}(\mathbf{r}) - \mathbf{v}(\mathbf{r}')]^2 d\mathbf{r}' \end{aligned} \quad (2.14)$$

The first term corresponds to a classical Lennard-Jones type two-body interaction between helium atoms. The interaction is screened at short distances where the interaction energy is of the same order as the correlation effects:

$$V_{LJ}(r) = \begin{cases} \epsilon_{LJ} \left[\left(\frac{\sigma}{r} \right)^{12} - \left(\frac{\sigma}{r} \right)^6 \right] & \text{if } r > h \\ 0 & \text{otherwise} \end{cases} \quad (2.15)$$

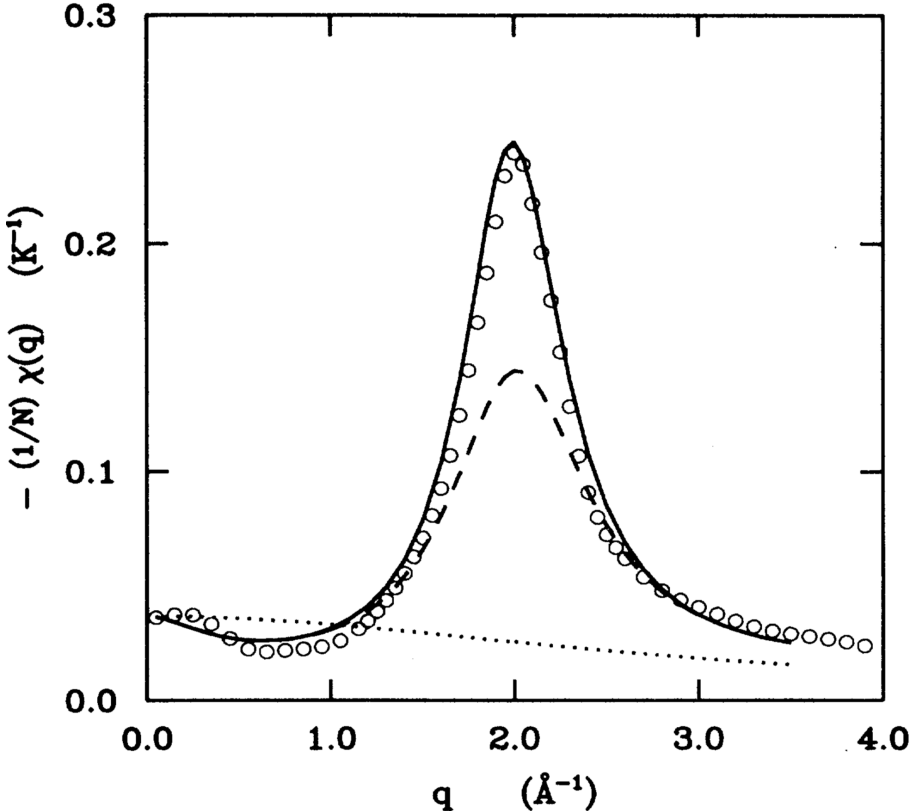


Figure 2.1: Static response $-\chi$ (see Ref. [29], Eqn. (11)) per atom of liquid ^4He at zero pressure. Points: experimental data; dotted line: from the functional of Refs. [50, 51]; dashed line: Orsay-Paris (OP) functional^[56]; solid line: OT functional.

In the second line, the terms corresponding to c_2 and c_3 , correct for short range correlations when $r < h$. The weighted density $\bar{\rho}$ is the average density ρ over a sphere of radius h :

$$\bar{\rho}(\mathbf{r}) = \int \Pi_h(|\mathbf{r} - \mathbf{r}'|) \rho(\mathbf{r}') d\mathbf{r}', \quad (2.16)$$

with

$$\Pi_h(r) := \begin{cases} \frac{3}{4\pi h^3} & \text{if } r \leq h \\ 0 & \text{otherwise} \end{cases} \quad (2.17)$$

The third line is a non-local correction to the kinetic energy (KC). It partially accounts for the difference $\mathcal{T}[\rho] - T[\rho]$ mentioned in Section 2.1. The gradient-gradient interaction function F is a Gaussian kernel defined as

$$F(r) = \frac{1}{l^3 \sqrt{\pi^3}} e^{-r^2/l^2} \quad (2.18)$$

All the parameters are fitted to reproduce the peak of the static response function (see Figure 2.1) in the bulk liquid. The factor $(1 - \tilde{\rho}/\rho_{0s})$ is included to match the pressure dependence of the static response function predicted by diffusion Monte Carlo calculations^[57]. The quantity $\tilde{\rho}(\mathbf{r})$ is another weighted density, calculated using

F as a weight

$$\tilde{\rho}(\mathbf{r}) := \int F(|\mathbf{r} - \mathbf{r}'|) \rho(\mathbf{r}') d\mathbf{r}' \quad (2.19)$$

The density $\tilde{\rho}(\mathbf{r})$ is very close to the normal density $\rho(\mathbf{r})$ except in very inhomogeneous situations. For helium droplets and free helium surfaces one can safely use ρ instead of $\tilde{\rho}$. In the presence of significant short-range density oscillations, e.g. in the presence of heavy atomic impurities as presented in this thesis or electrons, the helium density needs to be smoothed by the Gaussian kernel F .

Finally, the last line in Equation (2.14) is called the *back-flow* term and influences the dynamic response of the system. It plays the role of a non-local kinetic energy. Since the back-flow contains the factor $\mathbf{v} - \mathbf{v}'$, as defined in Equation (1.29) the contribution will only be non-zero whenever the effective wave function Ψ is complex-valued. Consequently, for time-independent case it means that this will only affect the vortex states. The phenomenological effective current-current interaction $V_J(r)$ is calibrated so that it reproduces the experimental phonon-roton spectrum (see Figure 1.3):

$$V_J(r) = (\gamma_{11} + \gamma_{12} r^2)e^{-\alpha_1 r^2} + (\gamma_{21} + \gamma_{22} r^2)e^{-\alpha_2 r^2} \quad (2.20)$$

All the parameters of the functional are given in Table 2.1.

2.2.1 THE SOLID-OT DENSITY FUNCTIONAL

In the presence of highly inhomogeneous liquid densities, e.g. atomic impurities with a very strong He-X interaction, the OT-functional Equation (2.14) becomes numerically unstable. To deal with this problem an additional cut-off can be used

$$\mathcal{E}^{\text{sol}} := C\rho(\mathbf{r})\{1 + \tanh(\beta[\rho(\mathbf{r}) - \rho_m])\} \quad (2.21)$$

where the model parameters $\{C, \beta, \rho_m\}$ are specified in Table 2.1. Including this term in the OT-functional prevents excessive density build-up. \mathcal{E}_{sol} only starts to deviate from zero whenever the liquid density ρ is comparable to ρ_m or larger. Therefore, inclusion of this term in the functional does not alter the density distribution. This penalty term was originally developed to account for the liquid-solid phase transition of ${}^4\text{He}$ ^[58,59]. The functional that has been used to obtain the result presented in this work is referred to as the “Solid-OT-DFT functional”. It consists of the first three terms of the original OT-functional Equation (2.14), plus E^{sol}

$$\begin{aligned} \mathcal{E}_c^{\text{sol}}[\rho] &= \frac{1}{2} \int \left\{ \rho(\mathbf{r}) V_{LJ}(|\mathbf{r} - \mathbf{r}'|) \rho(\mathbf{r}') \right. \\ &\quad \left. + \frac{1}{2} c_2 \rho(\mathbf{r}) [\bar{\rho}(\mathbf{r})]^2 + \frac{1}{3} c_3 \rho(\mathbf{r}) [\bar{\rho}(\mathbf{r})]^3 \right\} d\mathbf{r}' \\ &\quad + C \rho(\mathbf{r}) \{1 + \tanh(\beta[\rho(\mathbf{r}) - \rho_m])\} \end{aligned} \quad (2.22)$$

2.3 STATIC CALCULATIONS

In the work presented here all the impurities are heavy compared to the mass of ${}^4\text{He}$, e.g. the mass of Rubidium is about 21 times larger than that of Helium, Xenon roughly 33 times and Argon about 10 times. Therefore we will treat the centre of mass motion of the impurities as classical. In the functional this will be modelled as an external field V_X , the impurity-He pair interaction

$$E[\rho] \rightarrow E[\rho] + \int \rho(\mathbf{r}) V_X(|\mathbf{r} - \mathbf{r}_I|) d\mathbf{r} \quad (2.23)$$

where \mathbf{r}_I is the location of the impurity. Varying the modified functional to minimise the energy one now finds a new EL-equation in which the helium–impurity interaction is included:

$$\left\{ -\frac{\hbar^2}{2m_4} \nabla^2 + \frac{\delta \mathcal{E}_c}{\delta \rho} + V_X(|\mathbf{r} - \mathbf{r}_I|) \right\} \Psi(\mathbf{r}) = \mu \Psi(\mathbf{r}) \quad (2.24)$$

This equation is then solved by iteration in a self-consistent way by the imaginary time propagation method^[60] (ITM) in cartesian coordinates. The calculations are performed in three dimensions without imposing any symmetries that are present in the external potential. All the quantities are discretised on an evenly spaced Cartesian grid with a step-size that is typically of the order of 0.4 Å. The differential operators are evaluated using a k -point finite difference method where in most applications $k = 13$ is sufficiently accurate. The integrals in the density-functional can be expressed as convolutions and can therefore be evaluated in momentum-space by exploiting the convolution theorem, using proprietary highly optimised parallel Fast Fourier Transform algorithms.

2.3.1 PRODUCING VORTICAL STATES

The helium density that minimises the energy of the vortical states Ψ_s (Equation (1.30)), introduced in Section 1.2.4, can be obtained by solving the same EL-equation as for a vortex-free droplet. This becomes clearer when we write Equation (2.13) in cylindrical coordinates:

$$\left\{ -\frac{\hbar^2}{2m} \left[\frac{1}{r} \frac{\partial}{\partial r} \left(r \frac{\partial}{\partial r} \right) - \frac{s^2}{r^2} \right] + \frac{\delta \mathcal{E}_c}{\delta \rho} \right\} \Psi_s(\mathbf{r}) = \mu \Psi_s(\mathbf{r}) \quad (2.25)$$

Written like this it is evident that the ground state Ψ_0 is just the special case for $s = 0$. Obtaining the solution using the ITM works as long as the solution has overlap with initial guess for the order parameter. Starting with a trial order parameter similar to Ψ_s will guarantee this. To do this we use the “imprinting” technique where we use the ground state density of a previously obtained vortex-free droplet and multiply it with a normalised complex factor

$$\Psi(\mathbf{r}) = \sqrt{\rho_0(\mathbf{r})} \times \frac{x + iy}{\sqrt{x^2 + y^2}} \quad (2.26)$$

where ρ_0 is the ground state density of the vortex-droplet. In cylindrical coordinates this factor is equivalent to the one in Equation (1.30) for $s = 1$.

This changes for droplets with two or more vortices, where the cylindrical symmetry is broken and the solutions are no longer solutions of Equation (2.25), nor eigenfunctions of the angular momentum operator. In this case the time-independent EL-equation has to be modified to include a rotational constraint solution in the co-rotating frame

$$\mathcal{H} \rightarrow \mathcal{H} - \Omega \hat{L}_z \quad (2.27)$$

such that for a suitable choice of Ω the vortex-array solution becomes favourable to the ground state and also to excited states with angular momentum $s \geq 2$. Since these states are no longer eigenstates of the original time-dependent Hamiltonian, these states are no longer stationary and will start to rotate with frequency Ω . The initial guess for a droplet with n_v vortices can be produced using the same imprinting method as mentioned before

$$\Psi(\mathbf{r}) = \sqrt{\rho_0(\mathbf{r})} \times \prod_{j=1}^{n_v} \left[\frac{(x - x_j) + i(y - y_j)}{\sqrt{(x - x_j)^2 + (y - y_j)^2}} \right] \quad (2.28)$$

where ρ_0 is again the ground state density of the vortex-free droplet and (x_j, y_j) is the initial position of the j -th vortex-line parallel to the z -axis.

2.4 DYNAMIC CALCULATIONS

For the dynamic evolution of atomic impurities excited from ns -states to $n's$ -states, we do not need to keep track of the evolution of the electronic state of the impurity since it keeps its spherically symmetric orbital. In this case we only need to describe the time evolution of the centre of mass coordinate of the impurity. As in the statics, because of the large atomic mass of the impurity compared to helium, the time evolution of the centre of mass coordinate of the impurity is treated classically. To obtain the correct energy for the whole droplet-impurity system the energy functional needs to be extended to include the impurities centre of mass motion and the impurity-helium interaction

$$E[\rho] \rightarrow E[\rho] + \frac{p_I^2}{2m_I} + \int \rho(\mathbf{r}) V_{X^*}(|\mathbf{r} - \mathbf{r}_I|) d\mathbf{r} \quad (2.29)$$

where p_I is the classical momentum of the impurity, m_I is the impurity mass and V_{X^*} is the impurity-He pair interaction potential for an impurity in the ground-, excited $n's$ - or ionised state. The equations of motion for the time evolution of the effective wave function $\Psi(\mathbf{r}, t)$ and the second time derivative of the impurity location $\ddot{\mathbf{r}}_I$ are

$$\begin{aligned} i\hbar \frac{\partial}{\partial t} \Psi &= \left[-\frac{\hbar^2}{2m_4} \nabla^2 + \frac{\delta \mathcal{E}_c}{\delta \rho} + V_{X^*}(|\mathbf{r} - \mathbf{r}_I|) \right] \Psi \\ m_I \ddot{\mathbf{r}}_I &= -\nabla_{\mathbf{r}_I} \left[\int \rho(\mathbf{r}) V_{X^*}(|\mathbf{r} - \mathbf{r}_I|) d\mathbf{r} \right] \\ &= - \int V_{X^*}(|\mathbf{r} - \mathbf{r}_I|) \nabla \rho(\mathbf{r}) d\mathbf{r} \end{aligned} \quad (2.30)$$

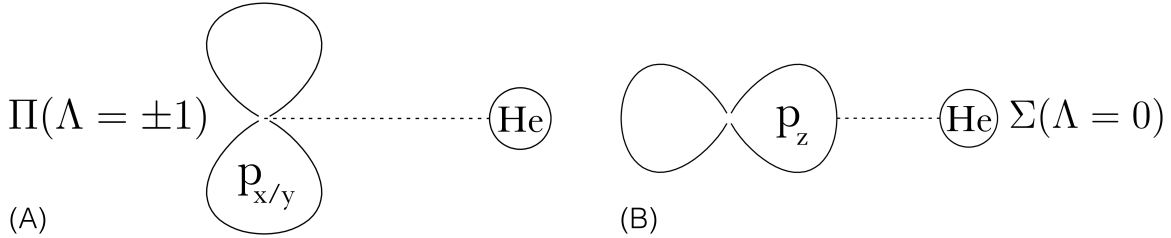


Figure 2.2: Level splitting of the p-orbitals in the presence of helium, that breaks the spherical symmetry. (A) A double degenerate $n'p_{x/y}$ -orbital and (B) a single $n'p_z$ -orbital. (Illustration courtesy of M. Martinez^[61].)

2.4.1 THE DIATOMIC MODEL

The situation becomes slightly more complicated for ns -states excited to $n'p$ -states (effective one-electron excited 2P -states). Since the three p-orbitals are no longer spherically symmetric and start mixing due to the interaction with the He droplet, we also need to include a description that accounts for the mixing of these orbitals in a dynamic way. To do this we use the diatomic model^[62] (DIM). The interaction between a helium atom (1S_0 -state) and the triple degenerate $L = 1$ electronic state of the impurity partially lifts the degeneracy so that the interaction can be decomposed into a Σ -state and a double degenerate Π -state (see Figure 2.2). In the cylindrical symmetry of the DIM it is customary to use the molecular term symbol ${}^{2S+1}\Lambda_\Omega$ to label the levels instead of ${}^{2S+1}L_J$. In the bound region of the potentials S is the electronic spin angular momentum (and $2S + 1$ the spin multiplicity), Λ is the modulus of the electronic orbital angular momentum and Ω is the total electronic angular momentum, all projected along the internuclear axis. Or symbolically

$$\mathbf{J} = \mathbf{L} + \mathbf{S} \longrightarrow \boldsymbol{\Omega} = \boldsymbol{\Lambda} + \mathbf{S}. \quad (2.31)$$

Following the spectroscopic notation the orbitals corresponding to $\Lambda = 0, 1, 2, 3, \dots$ are labeled $\Sigma, \Pi, \Delta, \Phi, \dots$. The interaction between a helium atom and the impurity's electronic structure can be expressed in an uncoupled basis

$$|p_{im}\rangle \in \{|p_{xm}\rangle, |p_{ym}\rangle, |p_{zm}\rangle\} \quad (2.32)$$

of real one-electron p-orbitals oriented along the internuclear axis (see Figure 2.3). The helium-impurity interaction matrix is given by

$$\begin{aligned} \mathcal{V}^{DIM}(r_m) &= V_\Pi(r_m)(|p_{xm}\rangle\langle p_{xm}| + |p_{ym}\rangle\langle p_{ym}|) + V_\Sigma(r_m)|p_{zm}\rangle\langle p_{zm}| \\ &= V_\Pi(r_m)(\mathbb{1}_3 - |p_{zm}\rangle\langle p_{zm}|) + V_\Sigma(r_m)|p_{zm}\rangle\langle p_{zm}| \\ &= V_\Pi(r_m)\mathbb{1}_3 + [V_\Sigma(r_m) - V_\Pi(r_m)]|p_{zm}\rangle\langle p_{zm}| \end{aligned} \quad (2.33)$$

where r_m is the modulus of the interatomic separation vector and V_Π and V_Σ are the Π and Σ impurity-He pair potentials in the absence of spin-orbit coupling. For a system consisting of N helium atoms the total interaction energy is calculated by summing over all the contributions of the N individual ${}^4\text{He}-X$ contributions

$$\mathcal{U}^{DIM}(\mathbf{r}_I) = \sum_{m=1}^N \mathcal{V}^{DIM}(r_m) \quad (2.34)$$

It is more convenient to express the interaction in a basis common to all impurity-helium pairs, instead of a basis that depends on the particular impurity-helium pair chosen. To do this we apply a rotation $\mathcal{R}_m : \hat{\mathbf{z}}_m \mapsto \hat{\mathbf{z}} \propto \mathbf{r}_I$, so that the matrix corresponding to the m^{th} ${}^4\text{He}$ atom expressed in the common basis is given by

$$|p_{zm}\rangle\langle p_{zm}| = \mathcal{R}_m |p_z\rangle\langle p_z| \mathcal{R}_m^{-1} \quad (2.35)$$

It can be shown that the elements of this matrix in cartesian coordinates are of the form

$$\langle p_i | \mathcal{R}_m | p_z \rangle \langle p_z | \mathcal{R}_m^{-1} | p_j \rangle = \frac{r_{im} r_{jm}}{\|\mathbf{r}_m\|^2} \quad (2.36)$$

where $(i, j) \in \{x, y, z\}$. With these definitions we can write the matrix elements U_{ij}^{DIM} of the interaction energy \mathcal{U}^{DIM}

$$U_{ij}^{\text{DIM}}(\mathbf{r}_I) = \langle p_i | \mathcal{U}^{\text{DIM}} | p_j \rangle = \sum_{m=1}^N V_{ij}^{\text{DIM}}(r_m) \quad (2.37)$$

where

$$V_{ij}^{\text{DIM}}(r_m) := V_\Pi(r_m) \delta_{ij} + \left[V_\Sigma(r_m) - V_\Pi(r_m) \right] \frac{r_{im} r_{jm}}{\|\mathbf{r}_m\|^2} \quad (2.38)$$

are the matrix elements of \mathcal{V}^{DIM} expressed in the common basis. Since we are working with a continuous helium density $\rho(\mathbf{r})$ and not with discrete atoms the summation over N helium atoms in the previous expression is replaced by an integral over the density $\sum_m \rightarrow \int \rho(\mathbf{r}) d\mathbf{r}$. This finally gives for the matrix element U_{ij}^{DIM}

$$U_{ij}^{\text{DIM}}(\mathbf{r}_I) = \int \rho(\mathbf{r} + \mathbf{r}_I) V_{ij}^{\text{DIM}}(r) d\mathbf{r} \quad (2.39)$$

The eigenvalues $U_k^{\text{np}}(\mathbf{r}_I)$ of this real symmetric matrix define the potential energy curves (PECs) without spin-orbit coupling as a function of the distance between the surrounding helium and the impurity.

2.4.2 INCLUDING SPIN-ORBIT COUPLING

For the study of the alkali metal Rb in this work, the spin-orbit (SO) splitting of the energy levels is comparable to the splitting of the orbital angular momentum levels $\Lambda = 0$ and $\Lambda = \pm 1$ due to the interaction with the helium. Therefore the spin-orbit interaction needs to be included in the total interaction Hamiltonian.

The total electronic Hamiltonian is given by the sum of the DIM-interaction and the SO-interaction

$$\mathcal{H} = \mathcal{U}^{\text{DIM}} + \mathcal{V}^{\text{SO}}. \quad (2.40)$$

The SO-matrix is approximated by the atomic alkali one, which is approximated by

$$\mathcal{V}^{\text{SO}} = g \mathbf{L} \cdot \mathbf{S} = \frac{1}{2} g (\mathbf{J}^2 - \mathbf{L}^2 - \mathbf{S}^2) \quad (2.41)$$

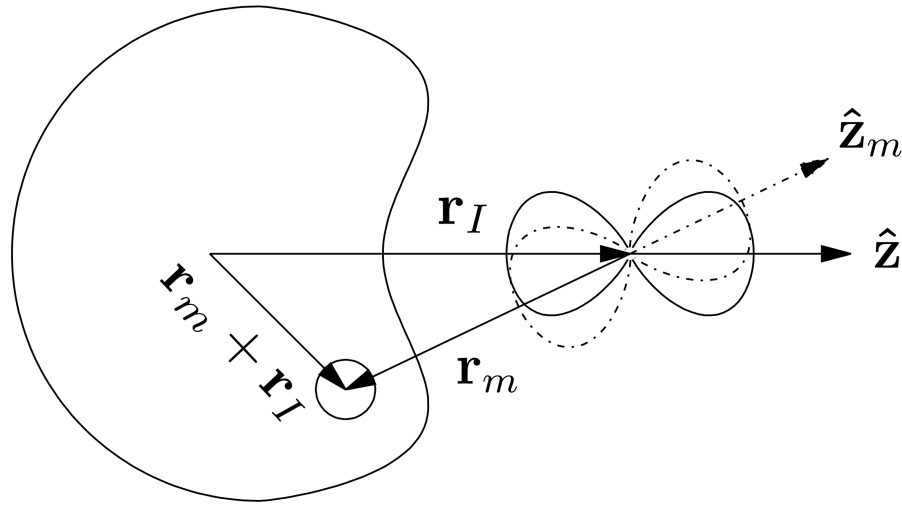


Figure 2.3: The set of axis defined in the DIM description. (Illustration courtesy of M. Martinez^[61].)

The coupling constant $A_{\ell s}$ is usually approximated by that of the free atom^[63]. We can extend the DIM basis Equation (2.32) to include the projection of the electron spin $s = \{\uparrow, \downarrow\}$ corresponding to the quantum numbers $m_s = \{\frac{1}{2}, -\frac{1}{2}\}$:

$$|p_i, s\rangle \in \{|p_x, \uparrow\rangle, |p_x, \downarrow\rangle, |p_y, \uparrow\rangle, |p_y, \downarrow\rangle, |p_z, \uparrow\rangle, |p_z, \downarrow\rangle\}. \quad (2.42)$$

In this basis the matrix \mathcal{V}^{SO} is given by

$$\mathcal{V}^{SO} = \frac{1}{2}g \begin{pmatrix} 0 & 0 & -i & 0 & 0 & 1 \\ 0 & 0 & 0 & i & -1 & 0 \\ i & 0 & 0 & 0 & 0 & -i \\ 0 & -i & 0 & 0 & -i & 0 \\ 0 & -1 & 0 & i & 0 & 0 \\ 1 & 0 & i & 0 & 0 & 0 \end{pmatrix} \quad (2.43)$$

Kramers' theorem states that the two-fold degeneracy of the levels originating from total half-integer spin cannot be broken by electrostatic interactions^[64]. Therefore all the electronic eigenstates of \mathcal{H} are doubly degenerate. Diagonalising \mathcal{H} yields three doubly degenerate PECs between the impurity and surrounding helium.

The dynamic evolution of the electronic excited state of the impurity is described by introducing an additional degree of freedom, a 6-component vector $|\lambda\rangle$, which describes the coefficients of the electronic state in the $\{|p_i, s\rangle\}$ basis

$$|\lambda(t)\rangle = \sum_{\substack{i=\{x,y,z\} \\ s=\{\uparrow,\downarrow\}}} \lambda_{is}(t) |p_i, s\rangle \quad (2.44)$$

such that $\|\langle\lambda|\lambda\rangle\|^2 = 1$. The complete set of variables required to describe the system consists of the complex valued effective wave function for helium $\Psi(\mathbf{r}, t)$ with $\rho(\mathbf{r}, t) = |\Psi(\mathbf{r}, t)|^2$, the impurity position $\mathbf{r}_I(t)$, and the 6-dimensional complex vector to determine its electronic wave function $|\lambda(t)\rangle$. The total energy of the impurity- ${}^4\text{He}_N$ complex after excitation to the ${}^2\text{P}$ manifold is

$$\begin{aligned} E[\Psi, \mathbf{r}_I, \lambda] &= \frac{\hbar^2}{2m} \int |\nabla \Psi|^2 d\mathbf{r} + \int \mathcal{E}_c[\rho] d\mathbf{r} \\ &\quad + \frac{p_I^2}{2m_I} + \int \rho(\mathbf{r}) V_\lambda(\mathbf{r} - \mathbf{r}_I) d\mathbf{r} + \langle \lambda | \mathcal{V}^{SO} | \lambda \rangle \end{aligned} \quad (2.45)$$

where V_λ is defined as

$$V_\lambda(\mathbf{r}) := \langle \lambda | \mathcal{V}^{DIM} | \lambda \rangle = \sum_{ijss'} \lambda_{is}^* V_{ijss'}^{DIM}(\mathbf{r}) \lambda_{js'} \quad (2.46)$$

and the components of the 6×6 matrix \mathcal{V}^{DIM} given by

$$V_{ijss'}^{DIM}(\mathbf{r}) = V_{ij}^{DIM} \delta_{ss'} = \left\{ V_{\Pi}(r) \delta_{ij} + [V_{\Sigma}(r) - V_{\Pi}(r)] \frac{r_i r_j}{\|\mathbf{r}_m\|^2} \right\} \delta_{ss'} \quad (2.47)$$

The time evolution of the system is obtained by minimising the following action

$$\begin{aligned} A[\Psi, \mathbf{r}_I, \lambda] &= \int \left\{ E[\Psi, \mathbf{r}_I, \lambda] - i\hbar \int \Psi^*(\mathbf{r}) \frac{\partial}{\partial t} \Psi(\mathbf{r}) d\mathbf{r} \right. \\ &\quad \left. - i\hbar \left\langle \lambda \left| \frac{\partial}{\partial t} \right| \lambda \right\rangle - \frac{1}{2} m_I \dot{\mathbf{r}}_I^2 \right\} dt \end{aligned} \quad (2.48)$$

Variation of the action A with respect to $\{\Psi^*, \langle \lambda |, \mathbf{r}_I\}$ yields the following three coupled EL-equations

$$\begin{aligned} i\hbar \frac{\partial}{\partial t} \Psi &= \left[-\frac{\hbar^2}{2m} \nabla^2 + \frac{\delta \mathcal{E}_c}{\delta \rho(\mathbf{r})} + V_\lambda(\mathbf{r} - \mathbf{r}_I) \right] \Psi \\ i\hbar \frac{\partial}{\partial t} | \lambda \rangle &= \mathcal{H} | \lambda \rangle \\ m_I \ddot{\mathbf{r}}_I &= -\nabla_{\mathbf{r}_I} \left[\int \rho(\mathbf{r}) V_\lambda(\mathbf{r} - \mathbf{r}_I) d\mathbf{r} \right] = - \int V_\lambda(\mathbf{r} - \mathbf{r}_I) \nabla \rho(\mathbf{r}) d\mathbf{r} \end{aligned} \quad (2.49)$$

where the explicit time dependence of the variables is omitted for clarity. The second line of Equation (2.49) is a 6×6 matrix equation with the matrix elements of \mathcal{H} given by

$$H_{ijss'} = U_{ijss'}^{DIM} + V_{ijss'}^{SO} = \int \rho(\mathbf{r}) V_{ijss'}^{DIM}(\mathbf{r} - \mathbf{r}_I) d\mathbf{r} + V_{ijss'}^{SO} \quad (2.50)$$

In the cases that SO-coupling can be neglected the 6-dimensional electronic state vector $| \lambda \rangle$ reduces to the 3-dimensional vector

$$| \lambda(t) \rangle = \sum_{i=\{x,y,z\}} \lambda_i(t) | p_i \rangle \quad (2.51)$$

and the 6×6 matrix \mathcal{H} reduces to the 3×3 matrix of Equation (2.39) with elements

$$H_{ij} = U_{ij}^{DIM} = \int \rho(\mathbf{r}) V_{ij}^{DIM}(\mathbf{r} - \mathbf{r}_I) d\mathbf{r} \quad (2.52)$$

For the technical details about how this method is implemented the interested reader is directed to Ref. [65]. For the collection of Fortran code that has been used to obtain the results presented here see Ref. [66]. For the manual to use the code, with included example calculations see Ref. [67].

3

ALKALI-DOPED NANODROPLETS

In their 1996 paper^[68] Griffin and Stringari have argued that almost 100% Bose-Einstein Condensation could be achieved in the low density surface region of superfluid He at $T = 0$, as opposed to only about 10% in the bulk. It is therefore evident that a minimally perturbing probe capable of investigating the surface of a He cluster is very desirable.

It was argued from a theoretical perspective^[69] that the alkali atoms reside on the cluster surface. Experimental evidence for this was found^[70–72] later when it was observed that the laser induced fluorescence (LIF) spectrum of sodium was shifted compared to sodium in the gas phase due to the presence of the He cluster. However, not as much as alkali atoms in the bulk of liquid helium.

It comes as no surprise then that alkali atoms are a very natural choice for exactly these type of studies. For example, with a solvation parameter (see Section 1.3) of $\lambda = 0.729$ ^[37], Rb will remain bound to the surface of the droplet. Furthermore, alkalis have a simple, well known, absorption spectrum. Moreover, their simple, one-valence electron structure allows for detailed theoretical modelling. They introduce only weak perturbations (alkali-helium interaction energies are on the order of 1 cm^{-1} ^[73]). Lastly, theoretical calculations^[74,75] and experimental spectra^[76–78] of alkali atoms in bulk liquid helium are available for comparison.

Surprisingly, the study of alkali atoms seeded in highly quantum matrices is relevant to the optimisation of the use of solid hydrogen as a rocket propellant^[79].

Given that alkalis are ideal objects to probe the boundary region of the nanodroplets, the $np\ ^2\text{P} \leftarrow ns\ ^2\text{S}$ transitions of the alkali atoms have attracted much interest from an experimental as well as a theoretical point of view. The spectroscopy of higher excited states has been thoroughly explored^[80–89]. The obtained spectra can be successfully reproduced by a pseudo-diatom model¹, except for the higher excited states, where the model progressively fails due to the limitations imposed by its realm of validity^[90,91]. While the effect of the excited states on the spectra are now fairly well understood, their influence on the following dynamics is largely unexplored.

¹Also called the “frozen droplet” model. It is equivalent to the DIM model, explained in Section 2.4.1, but where the internal structure of the droplet is neglected, i.e. the whole droplet is considered to be a single huge atom.

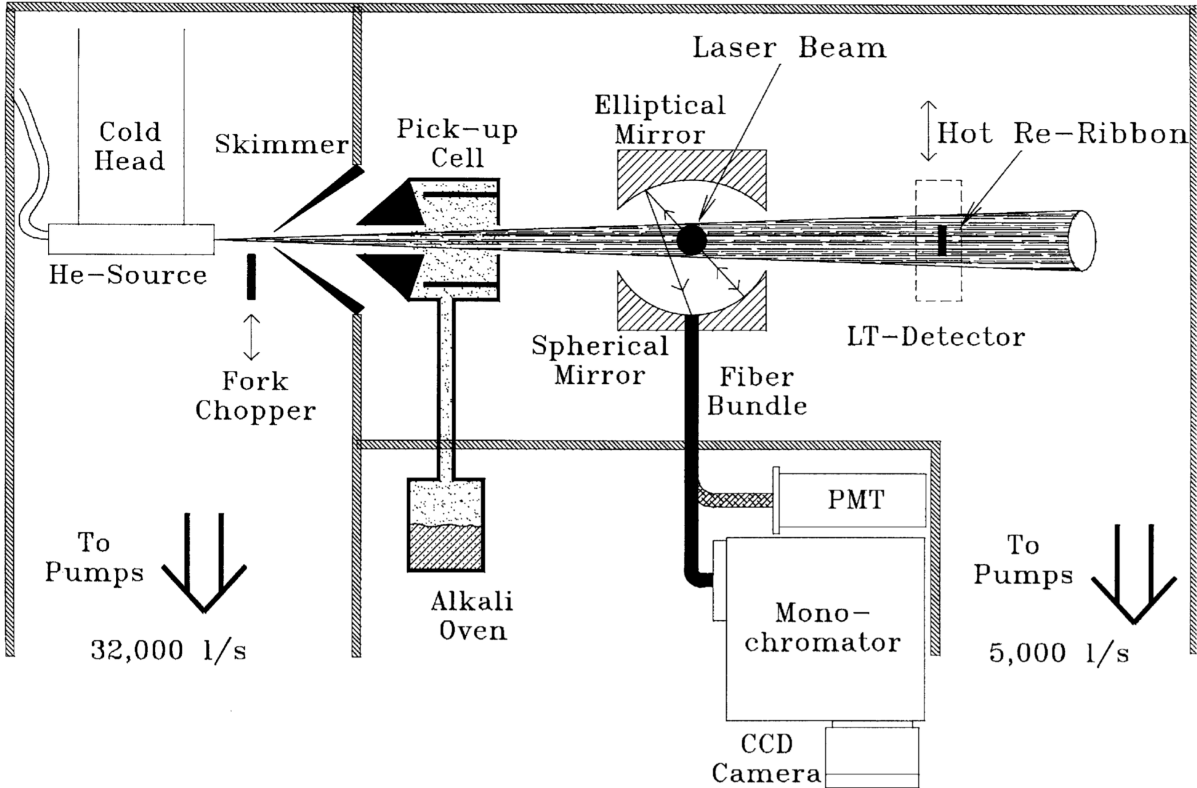


Figure 3.1: Principle of an alkali-doped helium nanodroplet experiment from Ref. [90]

In this part of the thesis, the results of the real-time dynamics of a single electronically excited rubidium (Rb) atom residing in the surface dimple of a helium nano-droplet are presented. The atom is excited from its ground state $5s^2\Sigma_{1/2}$ to the $5p^2\{\Sigma, \Pi\}$ and $6p^2\{\Sigma, \Pi\}$ manifold (see Section 2.4.1 for an explanation of the used electronic state labels). This is a combined experimental and theoretical study.

Experimental setup A beam of large He clusters is produced in a supersonic expansion from a cold nozzle (Figure 3.1). The weak He-He binding energy of 7.7 cm^{-1} [22] requires high stagnation pressures and low nozzle temperatures (T) for large cluster formation. For a set pressure, nozzle aperture and temperature the droplet sizes are log-normal distributed. Doping of the He clusters realised by sending the beam through a pick-up cell (located a short distance after the skimmer) in which a variable pressure of the alkali is maintained by connecting the pick-up cell with the reservoir through a heated tube. For a chosen average droplet size the average number of dopants picked-up by the droplet is governed by Poissonian statistics and can be controlled with the vapour pressure inside the pickup cell. In their path through the cell the larger clusters pick up alkali atoms without being appreciably deflected. Dissipation of the energy of the captured alkali is likely to occur by evaporation of He atoms from the clusters, the terminal temperature of which rapidly returns to its pre pick-up value ($\sim 0.4 \text{ K}$) [2].

To probe the picked-up alkali atoms a variety of measurement techniques can be employed, e.g. laser induced fluorescence (LIF) spectroscopy, time-resolved pump-probe spectroscopy, photo-electron spectroscopy and velocity map imaging (VMI).

The specific ones used in this work will be introduced generally in the next section.

4

QUANTISED VORTICES IN DROPLETS

ONE of the most unambiguous signatures of the quantum mechanical nature of a substance—and indeed superfluidity—is the appearance of quantised vortices. In contrast to a normal fluid, which will rotate as a solid body when its container moves at low angular velocity, a superfluid will remain at rest. However, above a certain critical angular velocity the thermodynamically stable state of a superfluid includes one or more quantum vortices. Such a vortex can be characterised by a macroscopic wave function and quantised velocity circulation in units of $\kappa = \frac{\hbar}{m}$, where \hbar is Planck's constant and m is the mass of the ^4He atom [2,3]. Recently, the study of vorticity was extended to finite systems such as BECs confined to traps [3,4]. The transfer of energy and angular momentum in finite systems between quantised vortices and surface excitations is of particular interest, as it defines the nucleation dynamics, shape, and stability of the involved vortices [3,4]. In comparison to confined BECs, ^4He droplets are self-contained and present a case for the strongly interacting superfluid. Moreover, the diameter of a vortex core which is approximately 0.2 nm in superfluid ^4He [2] is small relative to the droplet size, suggesting a three-dimensionality of the vortices in droplets. Vorticity in ^4He droplets has therefore attracted considerable interest [5–8].

A schematic of the experiment is shown in Fig. 4.1. Helium droplets are produced by expansion of He, at 20 bar and a temperature $T_0=5.4\text{--}7\text{ K}$, into vacuum through a nozzle of diameter $D = 1/4\text{--}5\text{ }\mu\text{m}$. The droplets cool rapidly via evaporation and reach a temperature of 0.37 K [20], which is well below the superfluid transition temperature $T_c = 1/4\text{--}2/17\text{ K}$ [2,3]. Further downstream, the droplets capture 103–106 Ag atoms in an oven [21]. The droplets are then collided against a thin carbon film substrate at room temperature [21]. Upon impact, the droplets evaporate, leaving on the surface the Ag traces, which are subsequently imaged via a transmission electron microscope (TEM).

Recently, Gomez, Loginov and Vilesov performed experiments[PRL 108, 155302 (2012)] where vortices inside superfluid ^4He droplets, produced by the expansion of liquid helium, were traced by introducing Ag atoms which clustered along the vortex lines, into the droplets. The Ag clusters were subsequently surface-deposited and imaged via electron microscopy. The prevalence of elongated track-shaped deposits (see Figure 1.5) shows that vortices are present in droplets larger than about 300 nm and that their lifetime exceeds a few milliseconds. Two years later Gomez reported[Science

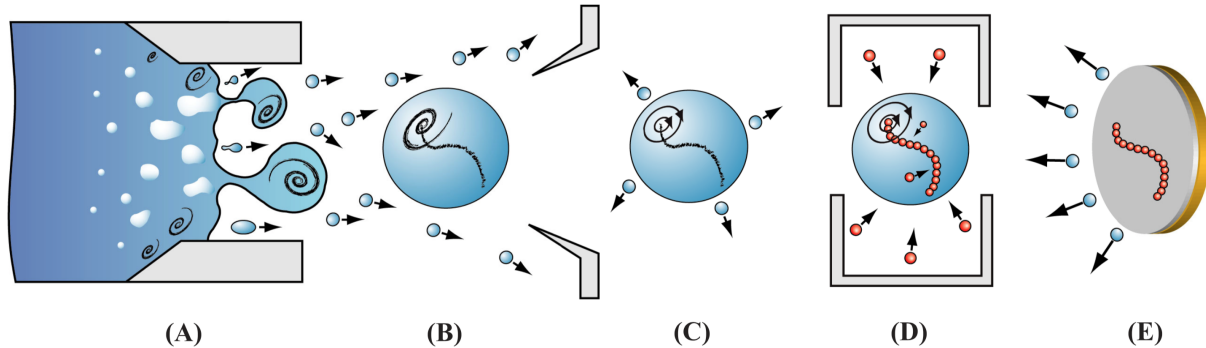


Figure 4.1: Schematic of the experiment. (a) He fluid expands in vacuum and (b) breaks up into rotating droplets. (c) A quantum vortex is formed as a consequence of fast evaporative cooling of the droplet to below T_λ . (d) The droplet is doped with Ag atoms, which are attracted to the vortex core. (e) The droplet then collides with the carbon surface leaving behind the Ag trace, whereas the He evaporates.

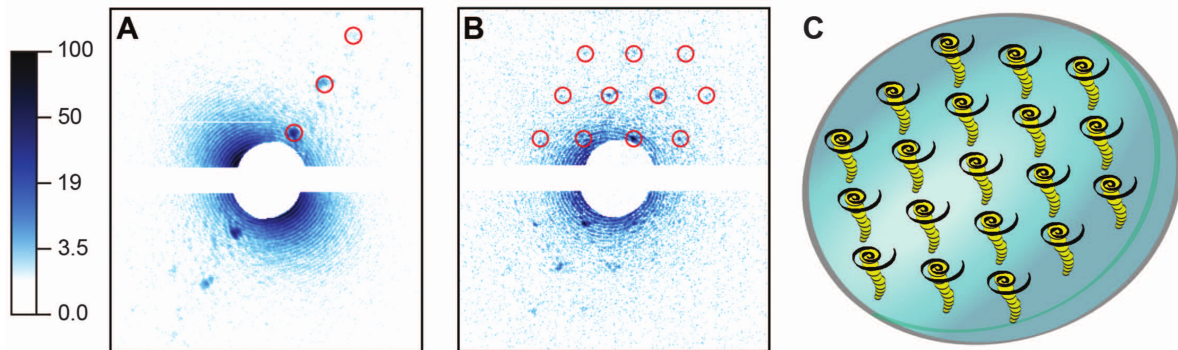


Figure 4.2: He droplets doped with Xe atoms. (A and B) X-ray diffraction images of doped droplets, displayed in a logarithmic intensity scale. (C) Droplet and embedded Xe clusters. Images in (A) and (B) correspond to tilted and parallel alignments of the vortex axes with respect to the incident x-ray beam, respectively.

345, 906 (2014)] on the formation of quantum vortex lattices inside droplets. He used single-shot femtosecond x-ray coherent diffractive imaging to investigate the rotation of single, isolated superfluid helium-4 droplets containing $\sim 10^8$ to 10^{11} atoms. The formation of quantum vortex lattices inside the droplets was confirmed by observing the characteristic Bragg patterns from xenon clusters trapped in the vortex cores (see Figure 4.2).

BIBLIOGRAPHY

- [1] P. Kapitza, *Nature* **141**, 74 (1938), URL <http://dx.doi.org/10.1038/141074a0>.
- [2] B. Rollin and F. Simon, *Physica* **6**, 219 (1939), ISSN 0031-8914, URL <http://www.sciencedirect.com/science/article/pii/S0031891439800131>.
- [3] W. Keesom and M. A. Keesom, *Physica* **3**, 359 (1936), ISSN 0031-8914, URL <http://www.sciencedirect.com/science/article/pii/S0031891436803127>.
- [4] L. Tisza, *Comptes rendus hebdomadaires des séances de l'Académie des sciences* **207**, 1035 (1938), URL <http://gallica.bnf.fr/ark:/12148/bpt6k31590/f1035.item>.
- [5] L. Tisza, *Comptes rendus hebdomadaires des séances de l'Académie des sciences* **207**, 1186 (1938), URL <http://gallica.bnf.fr/ark:/12148/bpt6k31590/f1186.item>.
- [6] L. Tisza, *J. Phys. Radium* **1**, 164 (1940), URL <https://doi.org/10.1051/jphysrad:0194000105016400>.
- [7] L. Tisza, *J. Phys. Radium* **1**, 350 (1940), URL <https://doi.org/10.1051/jphysrad:0194000108035000>.
- [8] P. Lebrun, *Cryogenics* **34**, 1 (1994), ISSN 0011-2275, fifteenth International Cryogenic Engineering Conference, URL <http://www.sciencedirect.com/science/article/pii/S0011227505800037>.
- [9] W. Keesom and M. A. Keesom, *KNAW, Proceedings* **35**, 736 (1932), URL <http://www.dwc.knaw.nl/DL/publications/PU00016277.pdf>.
- [10] R. J. Donnelly, *Physics Today* **62**, 34 (2009), <https://doi.org/10.1063/1.3248499>, URL <https://doi.org/10.1063/1.3248499>.
- [11] H. Kamerlingh Onnes, *KNAW, Proceedings* **10**, 744 (1908), URL <http://www.dwc.knaw.nl/toegangen/digital-library-knaw/?pagetype=publDetail&pId=PU00013699>.
- [12] H. Kamerlingh Onnes, *KNAW, Proceedings* **11**, 168 (1909), URL <http://www.dwc.knaw.nl/toegangen/digital-library-knaw/?pagetype=publDetail&pId=PU00013525>.
- [13] P. J. McLennan, H. Smith, and J. Wilhelm, *The London, Edinburgh, and Dublin Philosophical Magazine and Journal of Science* **14**, 161 (1932), <https://doi.org/10.1080/14786443209462044>, URL <https://doi.org/10.1080/14786443209462044>.

- [14] E. F. Burton, Nature **135**, 265 (1935), URL <http://dx.doi.org/10.1038/135265a0>.
- [15] M. v. Laue, F. London, and H. London, Zeitschrift für Physik **96**, 359 (1935), ISSN 0044-3328, URL <https://doi.org/10.1007/BF01343868>.
- [16] F. Simon, Nature **133**, 529 (1934), URL <http://dx.doi.org/10.1038/133529a0>.
- [17] F. London, Proceedings of the Royal Society of London A: Mathematical, Physical and Engineering Sciences **153**, 576 (1936), ISSN 0080-4630, <http://rspa.royalsocietypublishing.org/content/153/880/576.full.pdf>, URL <http://rspa.royalsocietypublishing.org/content/153/880/576>.
- [18] J. F. Allen, R. Peierls, and M. Zaki Uddin, Nature **140**, 62 (1937), URL <http://dx.doi.org/10.1038/140062a0>.
- [19] J. F. Allen and A. D. Misener, Nature **141**, 75 (1938), URL <http://dx.doi.org/10.1038/141075a0>.
- [20] F. London, Nature **141**, 643 (1938), URL <http://dx.doi.org/10.1038/141643a0>.
- [21] L. Tisza, Nature **141**, 913 (1938), URL <http://dx.doi.org/10.1038/141913a0>.
- [22] L. Landau, Phys. Rev. **60**, 356 (1941), URL <https://link.aps.org/doi/10.1103/PhysRev.60.356>.
- [23] L. Landau, Phys. Rev. **75**, 884 (1949), URL <https://link.aps.org/doi/10.1103/PhysRev.75.884>.
- [24] N. N. Bogolyubov, J. Phys. (USSR) **11**, 23 (1947), [Izv. Akad. Nauk Ser. Fiz. 11, 77 (1947)], URL <https://ufn.ru/ru/articles/1967/11/o/>.
- [25] E. A. Cornell and C. E. Wieman, Rev. Mod. Phys. **74**, 875 (2002), URL <https://link.aps.org/doi/10.1103/RevModPhys.74.875>.
- [26] W. Ketterle, Rev. Mod. Phys. **74**, 1131 (2002), URL <https://link.aps.org/doi/10.1103/RevModPhys.74.1131>.
- [27] L. Pitaevskii and S. Stringari, *Bose-Einstein Condensation and Superfluidity*, vol. 164 of *International Series of Monographs on Physics* (Oxford University Press, Great Clarendon Street, Oxford, OX2 6DP, United Kingdom, 2016), first edition ed., ISBN 978-0-19-875888-4, URL <http://dx.doi.org/10.1093/acprof:oso/9780198758884.001.0001>.
- [28] D. Mateo, M. Barranco, and J. Navarro, Phys. Rev. B **82**, 134529 (2010).
- [29] F. Dalfovo, A. Lastri, L. Pricaupenko, S. Stringari, and J. Treiner, Phys. Rev. B **52**, 1193 (1995), URL <https://link.aps.org/doi/10.1103/PhysRevB.52.1193>.
- [30] R. J. Donnelly, J. A. Donnelly, and R. N. Hills, J. Low Temp. Phys. **44**, 471 (1981).
- [31] D. M. Brink and S. Stringari, Zeitschrift für Physik D Atoms, Molecules and Clusters **15**, 257 (1990), ISSN 1431-5866, URL <https://doi.org/10.1007/BF01437187>.

- [32] M. Hartmann, R. E. Miller, J. P. Toennies, and A. Vilesov, Phys. Rev. Lett. **75**, 1566 (1995), URL <https://link.aps.org/doi/10.1103/PhysRevLett.75.1566>.
- [33] M. Hartmann, F. Mielke, J. P. Toennies, A. F. Vilesov, and G. Benedek, Phys. Rev. Lett. **76**, 4560 (1996), URL <https://link.aps.org/doi/10.1103/PhysRevLett.76.4560>.
- [34] M. V. R. Krishna and K. B. Whaley, The Journal of Chemical Physics **93**, 746 (1990), <https://doi.org/10.1063/1.459525>, URL <https://doi.org/10.1063/1.459525>.
- [35] S. A. Chin and E. Krotscheck, Phys. Rev. B **45**, 852 (1992), URL <https://link.aps.org/doi/10.1103/PhysRevB.45.852>.
- [36] E. Krotscheck and R. Zillich, The Journal of Chemical Physics **115**, 10161 (2001), <https://aip.scitation.org/doi/pdf/10.1063/1.1400780>, URL <https://aip.scitation.org/doi/abs/10.1063/1.1400780>.
- [37] F. Ancilotto, P. B. Lerner, and M. W. Cole, J. Low Temp. Phys. **101**, 1123 (1995).
- [38] S. Grebenev, J. P. Toennies, and A. F. Vilesov, Science **279**, 2083 (1998).
- [39] P. Sindzingre, M. L. Klein, and D. M. Ceperley, Phys. Rev. Lett. **63**, 1601 (1989).
- [40] M. V. Rama Krishna and K. B. Whaley, Phys. Rev. Lett. **64**, 1126 (1990), URL <https://link.aps.org/doi/10.1103/PhysRevLett.64.1126>.
- [41] M. Hartmann, N. Pörtner, B. Sartakov, J. P. Toennies, and A. F. Vilesov, The Journal of Chemical Physics **110**, 5109 (1999), <https://doi.org/10.1063/1.479111>, URL <https://doi.org/10.1063/1.479111>.
- [42] J. Harms, M. Hartmann, B. Sartakov, J. P. Toennies, and A. F. Vilesov, The Journal of Chemical Physics **110**, 5124 (1999), <https://doi.org/10.1063/1.479110>, URL <https://doi.org/10.1063/1.479110>.
- [43] M. Barranco, R. Guardiola, S. Hernández, R. Mayol, J. Navarro, and M. Pi, Journal of Low Temperature Physics **142**, 1 (2006), ISSN 1573-7357, URL <https://doi.org/10.1007/s10909-005-9267-0>.
- [44] F. Ancilotto, M. Barranco, F. Coppens, J. Eloranta, N. Halberstadt, A. Hernando, D. Mateo, and M. Pi, International Reviews in Physical Chemistry **36**, 621 (2017), <http://dx.doi.org/10.1080/0144235X.2017.1351672>, URL <http://dx.doi.org/10.1080/0144235X.2017.1351672>.
- [45] M. Mudrich and F. Stienkemeier, International Reviews in Physical Chemistry **33**, 301 (2014), <https://doi.org/10.1080/0144235X.2014.937188>, URL <https://doi.org/10.1080/0144235X.2014.937188>.
- [46] E. Krotscheck and J. Navarro, eds., *Microscopic approaches to quantum liquids in confined geometries*, vol. 4 of *Series on Advances in Quantum Many-Body Theory* (World Scientific, Singapore, 2002).
- [47] M. P. de Lara-Castells, G. Delgado-Barrio, P. Villarreal, and A. O. Mitrushchenkov, J. Chem. Phys. **125**, 221101 (2006).

- [48] M. P. de Lara-Castells, N. F. Aguirre, P. Villarreal, G. Delgado-Barrio, and A. O. Mitrushchenkov, *J. Chem. Phys.* **132**, 194313 (2010).
- [49] N. F. Aguirre, P. Villarreal, G. Delgado-Barrio, A. O. Mitrushchenkov, and M. P. de Lara-Castells, *Phys. Chem. Chem. Phys.* **15**, 10126 (2013).
- [50] S. Stringari and J. Treiner, *Phys. Rev. B* **36**, 8369 (1987).
- [51] S. Stringari and J. Treiner, *J. Chem. Phys.* **87**, 5021 (1987).
- [52] F. Dalfovo, A. Lastri, L. Pricaupenko, S. Stringari, and J. Treiner, *Phys. Rev. B* **52**, 1193 (1995).
- [53] P. Hohenberg and W. Kohn, *Phys. Rev.* **136**, B864 (1964), URL <https://link.aps.org/doi/10.1103/PhysRev.136.B864>.
- [54] W. Kohn and L. J. Sham, *Phys. Rev.* **140**, A1133 (1965), URL <https://link.aps.org/doi/10.1103/PhysRev.140.A1133>.
- [55] E. Runge and E. K. U. Gross, *Phys. Rev. Lett.* **52**, 997 (1984).
- [56] J. Dupont-Roc, M. Himbert, N. Pavloff, and J. Treiner, *Journal of Low Temperature Physics* **81**, 31 (1990), ISSN 1573-7357, URL <https://doi.org/10.1007/BF00683150>.
- [57] S. Moroni, D. M. Ceperley, and G. Senatore, *Phys. Rev. Lett.* **69**, 1837 (1992), URL <https://link.aps.org/doi/10.1103/PhysRevLett.69.1837>.
- [58] F. Ancilotto, M. Barranco, F. Caupin, R. Mayol, and M. Pi, *Phys. Rev. B* **72**, 214522 (2005).
- [59] F. Caupin, F. Ancilotto, M. Barranco, R. Mayol, and M. Pi, *J. Low Temp. Phys.* **148**, 731 (2007).
- [60] L. Lehtovaara, J. Toivanen, and J. Eloranta, *Journal of Computational Physics* **221**, 148 (2007), ISSN 0021-9991, URL <http://www.sciencedirect.com/science/article/pii/S0021999106002798>.
- [61] M. Martinez, Master's thesis, Université Toulouse III Paul Sabatier (2017), URL https://github.com/bcctl2016/M2Report-M_Martinez/blob/master/report/report.pdf.
- [62] F. O. Ellison, *Journal of the American Chemical Society* **85**, 3540 (1963), <https://doi.org/10.1021/ja00905a002>, URL <https://doi.org/10.1021/ja00905a002>.
- [63] Z. J. Jakubek, Q. Hui, and M. Takami, *Phys. Rev. Lett.* **79**, 629 (1997).
- [64] A. Nakayama and K. Yamashita, *J. Chem. Phys.* **114**, 780 (2001).
- [65] M. Barranco, F. Coppens, N. Halberstadt, A. Hernando, A. Leal, D. Mateo, R. Mayol, and M. Pi (2017), URL <https://github.com/bcctl2016/DFT-Guide/blob/master/dft-guide.pdf>.
- [66] M. Pi, F. Ancilotto, F. Coppens, N. Halberstadt, A. Hernando, A. Leal, D. Mateo, R. Mayol, and M. Barranco, *4HeDFT BCN-TLS* (2017), URL <https://github.com/bcctl2016/>.

- [67] F. Coppens, *4HeDFT BCN-TLS | User Manual* (2017), URL <https://github.com/bcntls2016/4hedft-bcntls-manual>.
- [68] A. Griffin and S. Stringari, Phys. Rev. Lett. **76**, 259 (1996), URL <https://link.aps.org/doi/10.1103/PhysRevLett.76.259>.
- [69] F. Dalfovo, Zeitschrift für Physik D Atoms, Molecules and Clusters **29**, 61 (1994), ISSN 1431-5866, URL <https://doi.org/10.1007/BF01437166>.
- [70] F. Stienkemeier, J. Higgins, W. E. Ernst, and G. Scoles, Zeitschrift für Physik B Condensed Matter **98**, 413 (1995), ISSN 1431-584X, URL <https://doi.org/10.1007/BF01338416>.
- [71] F. Stienkemeier, J. Higgins, W. E. Ernst, and G. Scoles, Phys. Rev. Lett. **74**, 3592 (1995), URL <https://link.aps.org/doi/10.1103/PhysRevLett.74.3592>.
- [72] F. Ancilotto, E. Cheng, M. W. Cole, and F. Toigo, Zeitschrift für Physik B Condensed Matter **98**, 323 (1995), ISSN 1431-584X, URL <https://doi.org/10.1007/BF01338398>.
- [73] S. H. Patil, J. Chem. Phys. **94**, 8089 (1991).
- [74] F. Ancilotto, G. DeToffol, and F. Toigo, Phys. Rev. B **52**, 16125 (1995), URL <https://link.aps.org/doi/10.1103/PhysRevB.52.16125>.
- [75] S. I. Kanorsky, M. Arndt, R. Dziewior, A. Weis, and T. W. Hänsch, Phys. Rev. B **50**, 6296 (1994), URL <https://link.aps.org/doi/10.1103/PhysRevB.50.6296>.
- [76] B. Tabbert, M. Beau, M. Foerste, H. Günther, C. Hönniger, H. Hust, K. Layer, G. zu Putlitz, and T. Schumacher, Zeitschrift für Physik B Condensed Matter **98**, 399 (1995), ISSN 1431-584X, URL <https://doi.org/10.1007/BF01338414>.
- [77] Y. Takahashi, K. Sano, T. Kinoshita, and T. Yabuzaki, Phys. Rev. Lett. **71**, 1035 (1993), URL <https://link.aps.org/doi/10.1103/PhysRevLett.71.1035>.
- [78] J. H. Beijersbergen, Q. Hui, and M. Takami, Physics Letters A **181**, 393 (1993), ISSN 0375-9601, URL <http://www.sciencedirect.com/science/article/pii/037596019390394F>.
- [79] P. Carrick, ed., *Theoretical Performance of Atomic and Molecular HEDM Additives to Solid H₂*, p. 412 (Proceedings of the High Energy Density Matter (HEDM) Contractor's Conference, Woods Hole, MA.; Edwards Air Force Base, CA, 1993), URL <http://www.dtic.mil/docs/citations/ADA274452>.
- [80] E. Loginov and M. Drabbels, Phys. Rev. Lett. **106**, 083401 (2011).
- [81] E. Loginov, C. Callegari, F. Ancilotto, and M. Drabbels, J. Phys. Chem. A **115**, 6779 (2011).
- [82] F. Lackner, G. Krois, M. Koch, and W. E. Ernst, The Journal of Physical Chemistry Letters **3**, 1404 (2012), pMID: 26286790, <https://doi.org/10.1021/jz300381y>, URL <https://doi.org/10.1021/jz300381y>.

- [83] F. Lackner, G. Krois, and W. E. Ernst, Molecular Physics **111**, 2118 (2013), <https://doi.org/10.1080/00268976.2013.788792>, URL <https://doi.org/10.1080/00268976.2013.788792>.
- [84] M. Theisen, F. Lackner, and W. E. Ernst, J. Chem. Phys. **135**, 074306 (2011).
- [85] L. Fechner, B. Grüner, A. Sieg, C. Callegari, F. Ancilotto, F. Stienkemeier, and M. Mudrich, Phys. Chem. Chem. Phys. **14**, 3843 (2012).
- [86] A. Pifrader, O. Allard, G. Auböck, C. Callegari, W. E. Ernst, R. Hubert, and F. Ancilotto, J. Chem. Phys. **133**, 164502 (2010).
- [87] F. Lackner, G. Krois, M. Theisen, M. Koch, and W. E. Ernst, Phys. Chem. Chem. Phys. **13**, 18781 (2011).
- [88] M. Theisen, F. Lackner, F. Ancilotto, C. Callegari, and W. E. Ernst, The European Physical Journal D **61**, 403 (2011), ISSN 1434-6079, URL <https://doi.org/10.1140/epjd/e2010-10504-5>.
- [89] F. Lackner, J. Poms, G. Krois, J. V. Pototschnig, and W. E. Ernst, J. Phys. Chem. A **117**, 11866 (2013).
- [90] F. Stienkemeier, J. Higgins, C. Callegari, S. I. Kanorsky, W. E. Ernst, and G. Scoles, Z. Phys. D **38**, 253 (1996).
- [91] O. Bünermann, G. Droppelmann, A. Hernando, R. Mayol, and F. Stienkemeier, The Journal of Physical Chemistry A **111**, 12684 (2007), pMID: 17997536, <https://doi.org/10.1021/jp0760760>, URL <https://doi.org/10.1021/jp0760760>.